



**Politecnico  
di Torino**

**POLITECNICO DI TORINO DIPARTIMENTO DI  
INGEGNERIA MECCANICA E AEROSPAZIALE  
(DIMEAS)**

**Master's Degree in Biomedical Engineering**

**A preliminary study for EEG-based BCI  
development for FES control**

**Supervisors**

**Prof. Danilo DEMARCHI**

**M.Sc. Fabio ROSSI**

**M.Sc. Andrea MONGARDI**

**Candidate**

**Manal EZZAHIRI**

**Luglio 2022**



## Abstract

The use of motor imagery to activate motor-related brain areas represents an effective tool for promoting motor rehabilitation in individuals with severe muscle deficits. The oscillations in neuronal activity occurring during motor imagery can be acquired and processed into external outputs by using Brain Computer Interface (BCI) systems. To improve the effectiveness of rehabilitation procedures, it is useful to combine BCI and a Functional Electrical Stimulation (FES) device, which takes as input the signal processed by the BCI and translates it into a stimulation that generates movement in the compromised limb. Indeed, an approach based on simultaneous activation of cortical regions (through motor imagery) and motor nerves of the muscle of interest (through FES) has the potential to promote functional reorganization of cortical structures, thereby improving the results of the rehabilitation procedure. Therefore, the development of new techniques for acquiring and processing neural activity to provide accurate inputs for FES activation plays a central role in the field of rehabilitation.

In this thesis work, two algorithms suitable for non-invasive BCIs applications were designed. The simplest signal recording method for BCI systems is ElectroEncephaloGraphy (EEG). EEG is a non-invasive technique that provides useful information to recognize the subject's motion intention, which is the event of interest for the activation of a FES device. The proposed algorithms process EEG signals recorded during motor imagery tasks, which are characterized by changes in cortical fluctuations in a specific frequency band, typical of the mu/alpha brain rhythm. These changes were detected by a threshold, iteratively determined and subject-specific, that defines the trigger event of motor intention. The first algorithm was developed with a standard approach and performs a signal analysis in the frequency domain. The parameter used in this procedure is the Power Spectral Density (PSD) of the signal, which shows amplitude suppression during motor imagination. The second algorithm was developed using a non-linear operator defined in the continuous domain, called Teager's Energy Operator (TEO), which tracks energy changes in the signal. Besides the threshold, in this approach an amplitude constraint was introduced to minimize the influence of artifacts and increase the accuracy of event recognition.

The goal of both implemented techniques was a fast, real-time detection of the motor intention events, and two different approaches were tested and compared, to assess which one provided the best performance in terms of sensitivity, specificity, accuracy, precision and activation delay. The tests were performed on two datasets, one provided by BCI competition IV and the other consisting of signals acquired on-site with g.tec HIamp recording system. To minimize processing complexity and

enable the development of a low-power and wearable system, the use of a single EEG channel was investigated. Application of the proposed methods to the on-site recorded dataset led to online accuracy rates of 83.7% for the PSD-based algorithm and 84.5% for the TEO-based one, while the movement onset detection latency was 410 ms and 1200 ms for the two approaches, respectively.



# Table of Contents

<b>Abstract</b>	I
<b>List of Tables</b>	IV
<b>List of Figures</b>	V
<b>1 Introduction</b>	1
1.1 Central Nervous System Anatomy and Function . . . . .	1
1.1.1 Brain and Spinal Cord Architecture . . . . .	2
1.1.2 Neurons Structure . . . . .	5
1.1.3 Generation and Propagation of Action Potential . . . . .	7
1.2 ElectroEncephaloGraphy (EEG) . . . . .	10
1.2.1 Neurophysiological origins of EEG Signal and Rhythms . . .	11
1.2.2 EEG signal Components Properties . . . . .	12
1.2.3 Acquisition Electrodes . . . . .	15
1.2.4 Acquisition Techniques . . . . .	16
1.3 Brain Computer Interface (BCI) . . . . .	18
1.3.1 Motor Imagery driven BCI . . . . .	18
1.3.2 FES-BCI System . . . . .	19
1.4 Movement Intention Detection . . . . .	20
1.4.1 Standard Approach . . . . .	20
1.4.2 Energy-based Approach . . . . .	22
<b>2 State of the Art</b>	24
2.1 FES-driven BCI Systems . . . . .	24
2.2 Single Channel EEG MI-based BCI Systems . . . . .	26
2.3 Wearable Systems . . . . .	27
<b>3 Algorithms Description</b>	28
3.1 Preliminary Assessments . . . . .	28
3.2 Power Spectral Density (PSD) based Algorithm . . . . .	31

3.2.1	Pre-processing . . . . .	31
3.2.2	Control Parameters . . . . .	33
3.2.3	Threshold Calibration . . . . .	35
3.3	Teager-Kaiser Energy Operator (TEO) based Algorithm . . . . .	38
3.3.1	Preprocessing . . . . .	38
3.3.2	TEO processed Signal . . . . .	40
3.3.3	Threshold and Amplitude Parameter Setting . . . . .	41
<b>4</b>	<b>Intervention Protocol Description</b>	<b>46</b>
4.1	Experimental Set-Up . . . . .	46
4.2	Cue-Based Motor Imagery Task . . . . .	48
<b>5</b>	<b>Experimental Results and Discussion</b>	<b>50</b>
5.1	Quantification Parameters . . . . .	50
5.2	PSD and TEO Methods Comparison . . . . .	56
<b>6</b>	<b>Conclusion and Future Perspective</b>	<b>64</b>
	<b>Bibliography</b>	<b>66</b>

# List of Tables

5.1	Quantitative results for the two algorithms obtained OFFLINE applied on Dataset 1 . . . . .	57
5.2	Quantitative results for the two algorithms obtained ONLINE applied on Dataset 1 . . . . .	57
5.3	Quantitative results for the two algorithms obtained OFFLINE applied on Dataset 2 . . . . .	60
5.4	Quantitative results for the two algorithms obtained ONLINE applied on Dataset 2 . . . . .	60

# List of Figures

1.1	Main components of Central Nervous System [1]. . . . .	1
1.2	Spinal Cord structure [2]. . . . .	2
1.3	The cortex is morphologically divided in four lobes: frontal, parietal, occipital and temporal. It is also organized in functional areas controlling sensory and cognitive functions [7]. . . . .	3
1.4	Subcortical regions [8]. . . . .	4
1.5	Six layers of cortex [9]. . . . .	5
1.6	Structure of a neuron [11]. . . . .	6
1.7	Types of neurons [11]. . . . .	7
1.8	The cell membrane potential is generated by diffusive and electric forces moving ions towards their equilibrium [11]. . . . .	8
1.9	Cell membrane potential shows depolarization, followed by repolarization and hyperpolarization, then returns to rest state [11]. . . . .	8
1.10	Result of summation of postsynaptic potentials. . . . .	10
1.11	The structure of pyramidal cells on the left and electric dipole of pyramidal cells on the right [15]. . . . .	11
1.12	The EEG signal results from the postsynaptic activity of the pyramidal neurons in the surface of the brain. Scalp potentials are particularly sensitive to dipoles of radially oriented pyramidal cells in the gyri [16]. . . . .	12
1.13	Brain rhythms [19]. . . . .	13
1.14	(A) Example of ERD/ERS time courses. (B) Maps of signal distribution on the scalp during motor imagery [23]. . . . .	14
1.15	Electrode placement on the scalp according to 10-20 International Standard System [27]. . . . .	16
1.16	Example of monopolar and bipolar EEG derivations [28]. . . . .	16
1.17	The motor Homunculus shows the effects of electrical stimulation of the cortex on human body parts [6]. . . . .	19
2.1	Schematic representation of BCI-FES system for neurorehabilitation [38]. . . . .	25

2.2	BCI-FES system developed in [41]. . . . .	26
2.3	g.NAUTILUS wearable EEG headset [44]. . . . .	27
3.1	Example of ERD/ERS calculation method [46]. . . . .	29
3.2	EEGLab Graphical User Interface to set the parameters to perform time-frequency analysis. . . . .	30
3.3	Time-frequency analysis performed on subject 1 during motor imagination task of both hands, second session. . . . .	31
3.4	ICA analysis of signals acquired from 25 electrodes from subject 3 of the BCI competition IV dataset . . . . .	32
3.5	Power Spectral Density of Subject 3 EEG data . . . . .	33
3.6	Power Spectral Density using Welch method for different window sizes. . . . .	34
3.7	Plot of the power content of Subject 1 EEG signal in time domain during motor imagery. The suppression of the power can be seen after the motor imagery task onset. . . . .	35
3.8	Iterative process to define a robust threshold for motor intention detection. . . . .	36
3.9	Time-controlled threshold. . . . .	37
3.10	Subject 5 power content signal. The power of the EEG signal (in blue) had to remain below the threshold for at least 1 second after the task onset (in black) to be identified as an event (in magenta). . . . .	37
3.11	[8-14]Hz Bandpass Butterworth filter transfer function . . . . .	38
3.12	Effect of the butterworth filter on the EEG signal. . . . .	39
3.13	Preliminary steps of processing of the EEG signal of Subject 5 during motor imagery task. . . . .	40
3.14	ROC curve of Subject 5 to determine the optimum value of k coefficient . . . . .	41
3.15	TEO signal of Subject 5. In magenta, the events detected by the first threshold block. . . . .	42
3.16	Example of high peak-to-peak amplitude noisy oscillations in Subject 5 TEO signal. . . . .	43
3.17	ROC curve for determining the maximum peak-to-peak amplitude of noisy oscillations. . . . .	44
3.18	Subject 5 TEO signal . . . . .	44
3.19	Steps of the TEO-based algorithm for motor intention detection. . . . .	45
4.1	International System 10-20. Electrodes highlighted are the ones employed in the acquisitions. . . . .	47
4.2	Electrode's placement on Subject 2 during on-site recording. . . . .	47
4.3	Experimental set-up. . . . .	47
4.4	Timing scheme of the paradigm. . . . .	48

4.5	Subject was instructed to watch the instruction on the screen and perform motor imagery till the cue disappeared. . . . .	49
5.1	Confusion Matrix (CM) presenting TP, FN, FP, TN values of TEO-based algorithm tested on Subject 1. . . . .	51
5.2	Normalized Confusion Matrix (NCM) presents the results in a more intuitive way, but the information related to the dataset (i.e. number of trials) is lost during normalization. . . . .	51
5.3	Example of TP detection from TEO-based signal of Subject 1. TP are defined when the system identifies the event after the onset of the task, while the cue is presented on the screen. . . . .	52
5.4	Example of TP detection from TEO-based signal of Subject 1. Even if two or more events are recognized, TP is counted only at the first activation during cue presentation. . . . .	52
5.5	Example of FP detection from TEO-based signal of Subject 2. FP is counted when the algorithm identifies an event in the period of time in which the blank screen is presented. . . . .	53
5.6	Example of FP detection from TEO-based signal of Subject 2. If two or more events are recognized during the rest period, all these events are counted as FP. . . . .	53
5.7	Example of FP detection from TEO-based signal of Subject 1. If the event (pointed by the arrow) was identified prior the onset of motor imagery, and continue during the time interval aimed at motor imagery, the event was not counted as FP . . . . .	54
5.8	Example of FP detection from TEO-based signal of Subject 1. The arrows point respectively a FN and a TN. . . . .	54
5.9	Example of TP detection from TEO-based signal of Subject 1. The activation delay is defined as the time between the onset of the motor imagery task and the instant when the first event is identified. . . .	56
5.10	Both algorithms shows a similar accuracy in recognizing movement intention detection. Accuracy of PSD-based method shows slightly higher inter-subjects variability. . . . .	58
5.11	TEO-based method tends to be slower than PSD-based one in the recognition on the brain activity changes induced by MI task. . . .	58
5.12	Accuracy of PSD-based algorithm during offline and online session.	59
5.13	Accuracy of TEO-based algorithm during offline and online session.	59
5.14	Both algorithms shows a similar accuracy in recognizing movement intention detection. Accuracy of PSD-based is slightly higher than TEO-based one. . . . .	61
5.15	TEO-based shows slower activation delay than PSD-based one in the recognition on the brain activity changes induced by MI task. . .	61

5.16 Accuracy of PSD-based algorithm during offline and online session.	62
5.17 Accuracy of TEO-based algorithm during offline and online session.	62
5.18 Accuracy of PSD-based algorithm obtained for different observation window lengths. . . . .	63

# Chapter 1

## Introduction

### 1.1 Central Nervous System Anatomy and Function

The nervous system is the major centre of control, regulation and communication of the body. It is divided in two main parts: the central nervous system (CNS), which coordinates and processes information from the entire body, and the peripheral nervous system (PNS), which consists of nerves that connect the central nervous system to the rest of the body (Figure 1.1).

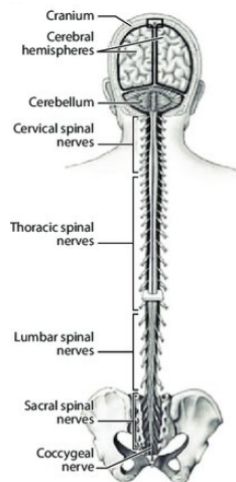


**Figure 1.1:** Main components of Central Nervous System [1].

### 1.1.1 Brain and Spinal Cord Architecture

The CNS comprises brain and spinal cord. The spinal cord is a tubular structure made of nervous tissue surrounded by vertebrae (Figure 1.2).

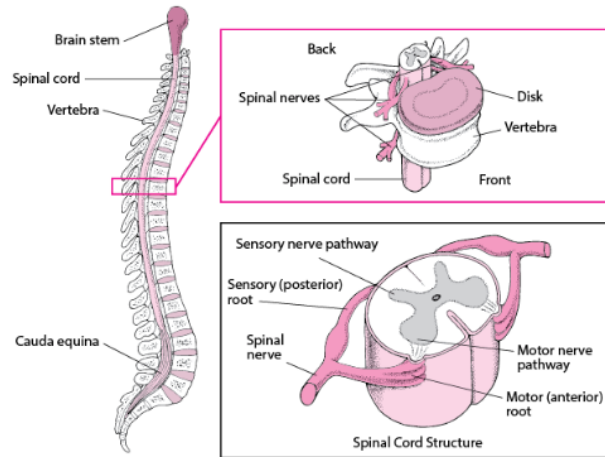


**Figure 1.2:** Spinal Cord structure [2].

It extends downwards from the brainstem to the lumbar region of the vertebral column. It plays a key role in the transmission of the sensory information, which are carried through the tightly packed column of axons, or nerve fibers, that make up the spinal cord. The axons of the sensory neurons that carry the information related to touch, position, pain and temperature run through the back side of the spinal cord, while the axons of the motor neurons, responsible for movement, run through the ventral part. Injuries to the spinal cord causes the loss of the perception and the ability to perform movements with the parts of the body served by the nerve fibers corresponding to the damaged regions [3, 4, 5]. Brain is the most complex organ of the human body and it is responsible for coordinating other organs functions, by processing and integrating sensory information through the nervous system. It is divided in three major regions: hindbrain, midbrain and forebrain. Hindbrain and midbrain together form the brainstem, while the forebrain comprises two symmetrical cerebral hemispheres. The surface of the brain is lined by the cerebral cortex, also called gray matter, because it contains most of the nerve cells, which give it its characteristic light gray color. Beneath the cortex are axons, i.e., extensions of neurons found in the cortex, which constitute the white matter. The cerebral cortex has a folded structure, developed to expand the total surface area of the brain, thus the space available for new neurons. The ridges are called gyrus and grooves are called sulcus. The cerebral cortex is divided into two hemispheres, and

each hemisphere is divided in four lobes: frontal, parietal, occipital and temporal (Figure 1.3). The hemispheres are characterized by contralateral organization, that means the motor and sensory functions of the right side of the body are controlled by the left hemisphere and vice-versa[6].

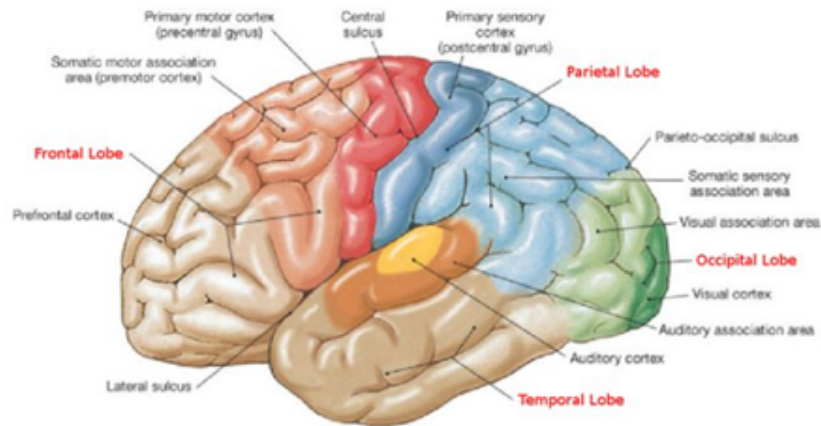


**Figure 1.3:** The cortex is morphologically divided in four lobes: frontal, parietal, occipital and temporal. It is also organized in functional areas controlling sensory and cognitive functions [7].

The frontal lobe is the most anterior part of the brain and plays a critical role in the control of voluntary movements, through two specific regions: primary motor cortex and pre-motor cortex. The primary motor cortex, located in the posterior area of the lobe, is responsible for controlling the movement of various body districts. In front of it the pre-motor cortex is located, which is responsible for organizing and controlling the movements of proximal muscles and of the torso. The other regions of the frontal lobe are involved in important cognitive functions such as long-term memory, emotions development, problem solving, social interaction and impulse control. The parietal lobe, located above the occipital lobe, processes information related to taste, touch and temperature and plays a central role in the development of the sense of space and position. The temporal lobe is located below the frontal and parietal lobes. It plays an important role in processing auditory stimuli and in developing language comprehension skills. The occipital lobe is located in the posterior part of the brain and it is responsible for processing visual information [3]. Subcortical areas of the brain are also important because they play a critical role in movement and sensory functions. The major regions that interact with cortex are: thalamus, brainstem, basal ganglia and cerebellum (Figure 1.4).

The thalamus, located below the cortex, serves as the main gateway to the cerebral cortex for sensory inputs from spinal cord and other subcortical structures. The brainstem lies at the base of the brain and contains motor and sensory nuclei, and also nerve fibers descending to and ascending from the spinal cord. The basal ganglia is a group of interconnected nuclei deeply involved in motor function. The cerebellum play an important role in the production of smooth and coordinated movements. The nervous tissue consists of neuronal cells, closely interconnected

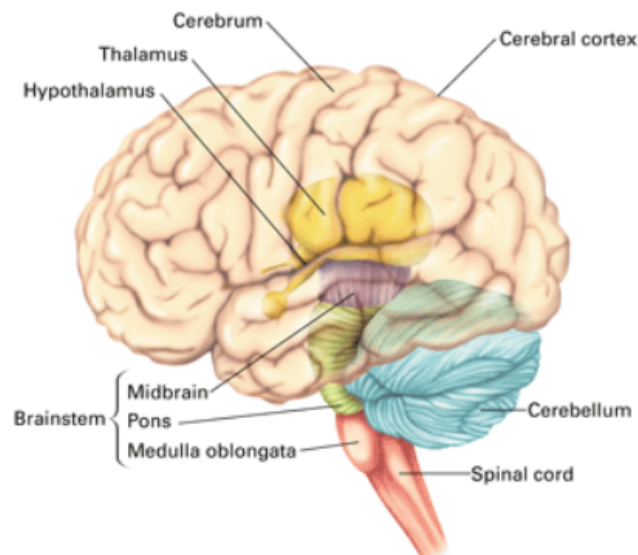


**Figure 1.4:** Subcortical regions [8].

by axons and dendrites, and glial cells, which act as support and protection for neurons and play an important role in the transmission of nerve impulses. The cerebral cortex consists of six layers, morphologically distinguishable by the type of cells they contain, which are mainly pyramidal cells and stellate cells, as well as horizontal and vertical nerve fibers, which connect different regions of the cortex and extend from the cortex to the spinal cord (Figure 1.5).

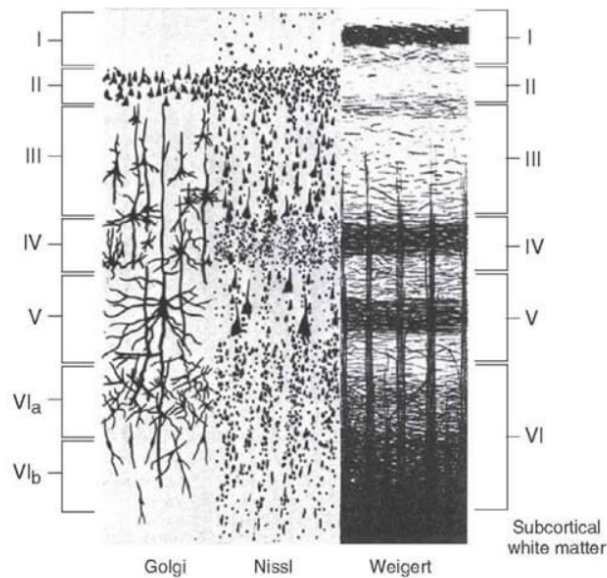


**Figure 1.5:** Six layers of cortex [9].

Layer I contains few neurons and consists mainly of dendrites extending from the apex of pyramidal cells to the deepest striae of the cortex and horizontally arranged fibers. Layer II contains stellate cells and smaller pyramidal cells. Layer III is the primary source of fibers that interconnect the different areas of the cortex. Layer IV includes the afferent fibers, which reach the cortex carrying sensory information. Layer V contains the larger pyramidal cells, which have long axons that act as efferent fibers and carry information outside the cortex. Finally, layer VI encloses a diverse collection of cells of different types [6, 10].

### 1.1.2 Neurons Structure

Neurons are specialized communication cells of the nervous system. They are responsible for the electrical signals that carry informations about internal and external state changes of the body and the activation of muscles and glands in response to those stimuli. The most important part of the neuron is the soma, or cell body, which includes the nucleus and major organelles, from which extensions called processes emerges. The most important process is the axon, which has the role of conducting electrical impulses from the cell body to the target cells. The neuron's other processes are called dendrites (Figure 1.6). Dendrites receive information from other neurons through specific contact areas called synapses, and conduct the impulse to the cell body, which processes the information and transmits it along the axon. The larger the surface area of dendritic membranes,

the greater the number of synapses the neuron can establish with other nerve cells [4]. Electrical signals are generated at the junction point of the axon with

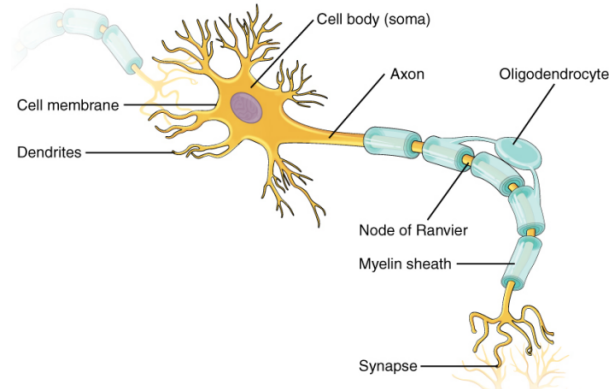


**Figure 1.6:** Structure of a neuron [11].

the cell body, which is called axon hillock, and from here the impulses descend along the axon, traveling along its entire length. The terminal part of the axon develops into branches, which allow neurons to communicate with more nervous cells. At the extreme apex of each branch is the axon terminal, a small expansion containing mitochondria and synaptic vesicles, which contain neurotransmitters. Many axons are covered with myelin, which is made of cytoplasmic extensions of glial cells. Myelin does not cover the entire axon: the axon hillock remains uncovered and there are gaps between myelinated segments, which are called nodes of Ranvier. The myelin covering has a central role in controlling both the timing and the insulation of the electrical signal as it runs down the axon. There are different criteria for classifying neurons, the most common involves a morphological classification based on the number of processes attached to the cell body (Figure 1.7). Pseudo-unipolar neurons have only one process departing from the cell body. These cells are generally located in the sensory and autonomic nervous systems. Bipolar neurons have two processes. They are not very common neurons, they are localized mainly in the retina of the eye. Finally, multipolar neurons are the most common cell type that can be found in the nervous system, and have many processes. These neurons are further distinguishable by their shape, for example, the cells in the cerebral cortex and hippocampus have triangular-shaped bodies, so they are called pyramidal cells, while the cells in the cerebellum have very extensive dendritic branches and are called Purkinje cells [11]. Neurons can also be classified according to their function in the nervous system. Sensory neurons receive information from the outside world, and these stimuli are translated into neuronal signals that are subsequently processed by the brain. Motor neurons are responsible for the transmission of CNS commands to muscles and glands. All

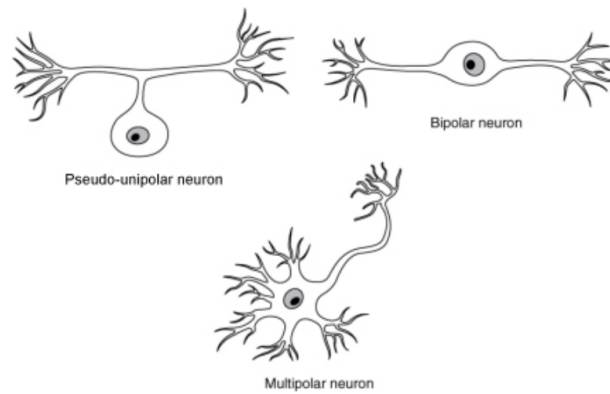


**Figure 1.7:** Types of neurons [11].

other neurons are interneurons, non-specialized cells that enable communication between motor and sensory neurons [12].

### 1.1.3 Generation and Propagation of Action Potential

Neuronal signals, or action potentials, are produced by ions moving across the neuronal membrane. This displacement occurs by diffusion, as there is a difference in the relative concentration of ions between intra- and extracellular fluid. Extracellular fluid is characterized by large concentrations of chloride ions ( $\text{Cl}^-$ ) and sodium ions ( $\text{Na}^+$ ), and a low concentration of potassium ions ( $\text{K}^+$ ). In contrast, intracellular fluid, in the resting neuron, contains a large amount of potassium ions and a low concentration of  $\text{Na}^+$  and  $\text{Cl}^-$  ions, as well as numerous negative particles, which contribute to amplifying the negative charge inside the cell. The potential difference between the inside and the outside of the cell turns out to be  $-70$  millivolt, and this difference, measured when the nerve cell is not active, is called the resting potential (Figure 1.8). Due to the difference between ion charges, another force that determines the displacement of ions is the electric force, which works in opposition to or in the same direction as diffusion, to constantly ensure the electrochemical balance of the cell. If the membrane potential moves away from the resting potential in a more positive direction, the membrane is in a state of depolarization. There is a threshold value that determines when a polarizing discharge is sufficient to trigger the sequence of events that generates the action potential, and this threshold corresponds to a depolarization of about  $-65$  millivolt. When the threshold is reached, voltage-gated sodium channels open. A voltage-gated channel is a structure that responds to changes in the electrical properties of the membrane in which it is embedded. In the case of depolarization, when the voltage within the cell becomes less negative, the channels open allowing

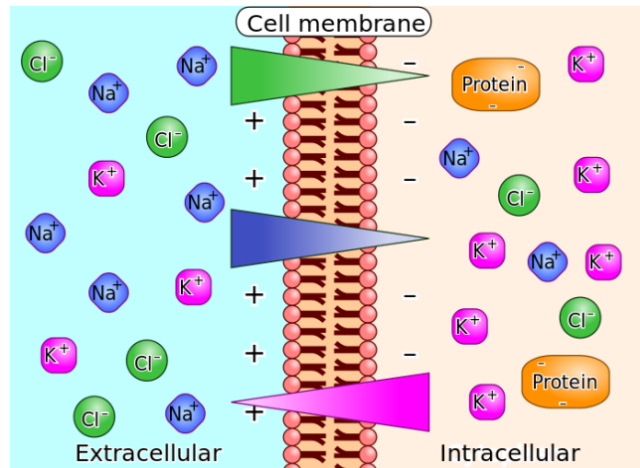


**Figure 1.8:** The cell membrane potential is generated by diffusive and electric forces moving ions towards their equilibrium [11].

the passage of ions. The entry of sodium ions into the cell brings to a rising of the potential from a threshold value of about -55 milliVolt to a maximum value that fluctuate around +40 milliVolt. When the peak of the action potential occurs in the cell, the environment inside the membrane is more positive than outside, so the sodium channels close and the voltage-gated potassium channels open, and potassium begins to leave the cell, causing the lowering of the potential. The potential go down beyond the resting state, causing a condition called hyperpolarization, which describes a change in the membrane potential in a more negative direction compared with the resting potential. After the closure of the voltage-gated potassium channels, the potential returns to the resting state (Figure 1.9). The

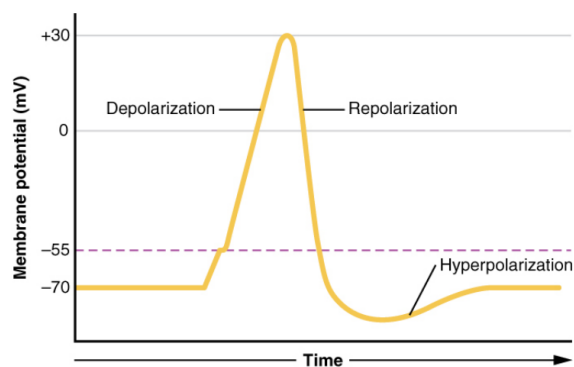


**Figure 1.9:** Cell membrane potential shows depolarization, followed by repolarization and hyperpolarization, then returns to rest state [11].

frequency of neural pulses generation is limited by the properties of the membrane channels. When the peak of the action potential is reached and the voltage-gated sodium channels close, a short refractory time follows in which the channels cannot re-open until the cell returns to the membrane potential, and no stimulus can trigger a new action potential. The refractory time prevents the generation of an impulse in a segment that has just produced one, and ensures the unidirectionality of action potential propagation, which travels from the soma to the axon terminal. Neural information does not depend on the intensity and the amplitude of the action potential, but follows the “All or Nothing” principle, that means it depends on the frequency of generation of action potentials. The greater the number of action potentials generated, the greater the intensity of the stimulus [11].

Propagation of the action potential occurs along the axon due to the presence of ion channels concentrated in the myelin sheath gaps, called Ranvier nodes. Myelination allows the action potential to jump between the Ranvier nodes, rather than requiring it to activate each segment between the two nodes. This type of conduction is called saltatory conduction and, because of myelin, it is faster and more efficient than the regular one [4]. Neurons transmit impulses to the other cells by two different mechanisms, electrical junctions and chemical synapses. The electrical junction is a direct connection between two active cells, in which ions can pass directly from one to the other. When one cell depolarizes, the joined cell also depolarizes, as ions diffuse between cells. Since the cells are joined by an ion channel, the signal can be transmitted in either direction. The chemical synapse is a gap where neurotransmitters are released to flow from the presynaptic neuron to the postsynaptic neuron, where neurotransmitters bind to specific receptors. In this case, the signal can only be transmitted in one direction, from the presynaptic cell to the postsynaptic cell. The binding between neurotransmitters and receptors in the postsynaptic cell can lead to the generation of an excitatory signal or an inhibitory signal. In the former case, the postsynaptic membrane receives a mild depolarization, called excitatory postsynaptic potential (EPSP). EPSPs are produced by the opening of ligand-gated sodium channels, controlled by a ligand (neurotransmitter) that binds to a specific location on the extracellular surface of the cell and causes the channel to open to allow  $\text{Na}^+$  ions to pass through. EPSPs are called graded potentials because they do not follow the all-or-nothing principle like the action potential. Ions emerging from the channel diffuse within the postsynaptic cell, and as their concentration in a given membrane segment dilutes, the voltage level in that segment changes. This means that the voltage gradually repolarizes with the distance of the ions from the channel, allowing the EPSP to vary in intensity. In the second case, neurotransmitter-receptor binding results in the generation of an inhibitory postsynaptic potential (IPSP). IPSP is a mild hyperpolarization of the postsynaptic membrane, which reduces the probability of the postsynaptic neuron to generate an action potential. IPSP is a graded

potential generated by the opening of ligand-gated chlorine and/or potassium channels, which allow chloride ions to enter the neuron or positive potassium ions to leave the cell to increase the negative charge within the cell. A neuron receives both excitatory and inhibitory impulses from multiple surrounding neurons. If the summation effect of all these signals causes the membrane to reach the threshold, then an action potential is generated. The summation can be achieved by two different mechanisms. The first one is called Spatial Summation, in which multiple synapses close to each other all activate at the same time, and the neuron adds up all the excitatory signals and subtracts the inhibitory ones. If the end result induces sufficient depolarization in the axon hillock, the cell generates an impulse (Figure 1.10). The second mechanism is called Temporal Summation, because it is the summation at a single synapse over a very short period of time of EPSP and IPSP. It results from a very rapid firing at the single synapse, so the membrane does not have the time to completely repolarize before the next signal arrives [11].

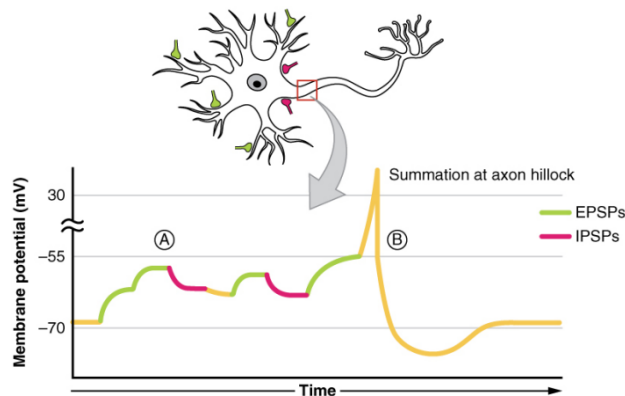


**Figure 1.10:** Result of summation of postsynaptic potentials. At point A, a summation of excitatory postsynaptic potentials add up to the depolarization. At point B, the total summation of excitatory and inhibitory postsynaptic potentials can be observed [11].

## 1.2 ElectroEncephaloGraphy (EEG)

ElectroEncephaloGraphy (EEG) is a non-invasive technique that records brain electrical activity by using electrodes placed over the scalp. Richard Charton (1842-1942) recorded the first EEG in cats and monkeys, using non-polarized electrodes and a mirror galvanometer. In 1924 Hans Berger recorded brain activity in humans for the first time, paving the way for the development of this technique, which is now widely used in clinical applications [13].

### 1.2.1 Neurophysiological origins of EEG Signal and Rhythms

The EEG signal is the spatial average of electric fields generated by pyramidal cell dendrites in the superficial layers of the cortex. These fields are due to the summation of excitatory postsynaptic potentials (EPSPs) and inhibitory potentials (IPSPs) of neuronal cell populations involved in synchronized activities. Pyramidal cells are disposed vertically to the surface of the cortex, with dendrites arranged parallel to each other. When the potential of the cell changes from that of an adjacent cell, an extracellular current flows from one cell to another, generating a measurable potential difference at the surface [11]. In this sense, pyramidal cells behave as dipole sources (Figure 1.11). These dipoles produce an external potential when they act synchronously, and this phenomenon is made explicit by Poisson's equation [14]:

$$\nabla (\theta \nabla (V)) = -J \quad (1.1)$$

Where  $V$  is the potential field,  $J$  is the current source density and  $\theta$  is the conductivity tensor.

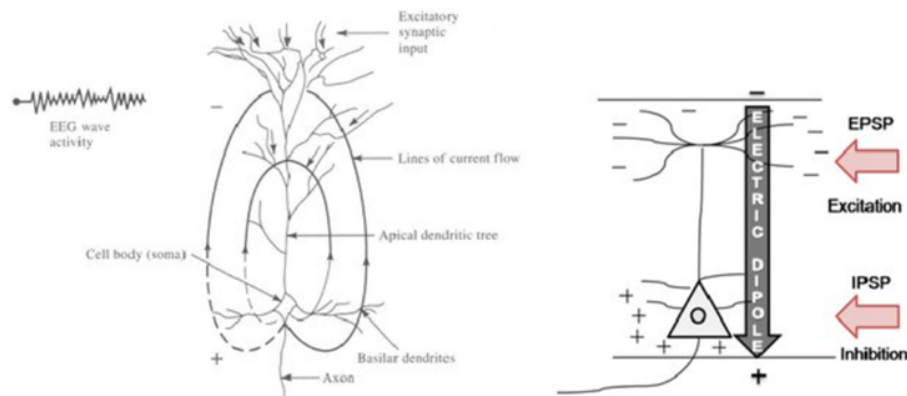


**Figure 1.11:** The structure of pyramidal cells on the left and electric dipole of pyramidal cells on the right [15].

The phenomenon of local synchrony, whereby a group of cortical cells depolarize in unison, is essential for recording brain activity. In fact, most pyramidal cells operate asynchronously, so their external potentials cancel each other out; however, if even a small portion of pyramidal cells polarize simultaneously, this will be visible in the EEG, as they generate a total field given by the linear combination of the potential fields that each source would produce individually. The location

of these dipoles also affects the EEG measurement. In fact, the cortical surface is characterized by folds and grooves, in which pyramidal cells perpendicular to the surface itself are located. Therefore, even if the sensor is located directly above the active site, it could detect no activity if the dipoles within the grooves are oriented horizontally with respect to each other. In that case the total potential will be zero. This phenomenon is called "paradoxical lateralization" (Figure 1.12).

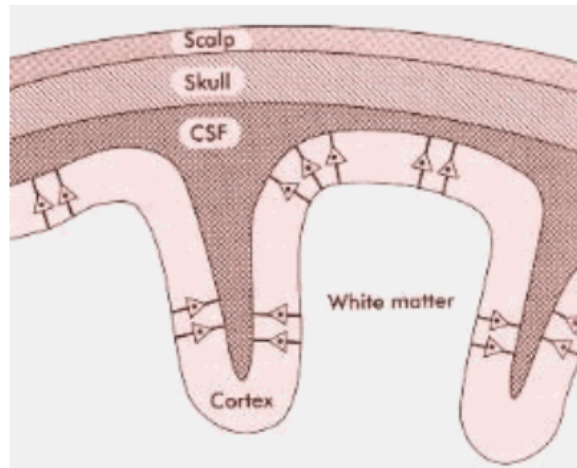


**Figure 1.12:** The EEG signal results from the postsynaptic activity of the pyramidal neurons in the surface of the brain. Scalp potentials are particularly sensitive to dipoles of radially oriented pyramidal cells in the gyri [16].

The extracellular current generated by each cell is extremely small, but this flow is propagated throughout the brain because of a phenomenon called "conduction volume". This phenomenon is due to the fact that tissues, which are made up mostly of water, are good conductors, and allow the passive propagation of electric current throughout the brain. Therefore localized brain activity spreads by conduction volume and may appear at more than one site in the scalp. However, conduction volume also causes the spread of non-neuronal physiological electrical signals, such as eye movements and muscle and heart activities, which inevitably affect the recorded EEG signal. Non-pyramidal cells in the cortex do not contribute significantly to surface signal recordings [10, 17].

### 1.2.2 EEG signal Components Properties

Neurons in the cortical area are organized into functional groups, closely interconnected by a dense network of links between cortical regions and subcortical structures. These groups of neurons are involved in cyclic activities necessary

for normal brain function, occurring in a frequency band ranging from 1 to 100 Hz and beyond. This coordinated activity, characterized by identifiable rhythmic waves, generates the recordable electrical signal, which is measured over time and shows high variability. The EEG signal shows a complex harmonic composition, characterized by distinguishable frequency components called rhythms. Typically, one particular component dominates over the others during a specific brain activity. Brain rhythms are defined by their location, amplitude, morphology, synchrony, symmetry and responsiveness, but the most common method of classifying these waves is by frequency [18]. Four main rhythms can be distinguished: delta waves ( $\delta$ ), beta waves ( $\beta$ ), theta waves ( $\theta$ ) and alpha waves ( $\alpha$ ). Gamma waves ( $\gamma$ ) may also be present on frequency bands greater than 40 Hz (Figure 1.13). Each rhythmic

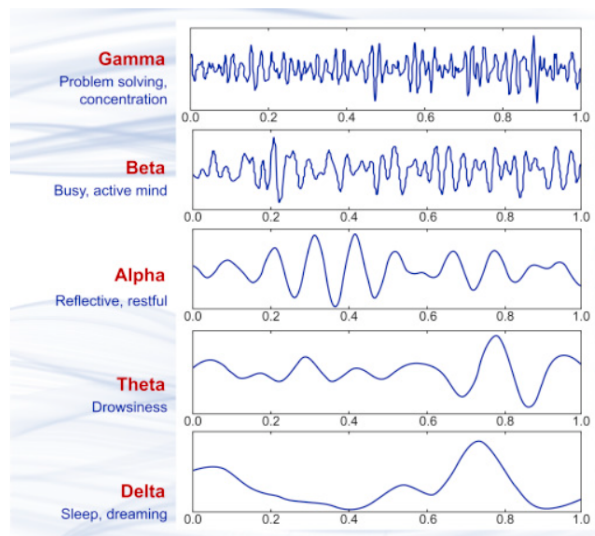


**Figure 1.13:** Brain rhythms [19].

wave is generated by specific interconnections. Alpha rhythm and slow beta rhythm are originated by a mechanism called thalamus-cortical resonance, due to the close connection between the thalamus and the adjacent cortical regions, which undergo thalamic resonance activity. Low-frequency theta waves are generated by resonance between the cortex and subthalamic nuclei, while beta waves, which are faster, are produced by short-range connections between cortical sites [20].

Delta waves have a bandwidth of 1-3 Hz and are associated with non-REM sleep states and states of unconsciousness. This rhythm excessively concentrated in a particular area is a symptom of severe dysfunction of that area, due to localized injury or trauma, for example. Excessive delta rhythm in a global area, on the other hand, indicates generalized pathology, aging, and other systemic problems [21].

The alpha rhythm have a frequency ranging from 8 to 13 Hz. It is a rhythm that reach its maximum intensity in the posterior area of the brain, and tends to increase during relaxation of the visual system. This happens because the alpha wave is a thalamo-cortical resonance that involve the optic pathways and primary visual cortex. During concentrated alpha activity, the individual is relaxed but conscious, so an increase in alpha waves represents less brain activity [20]. The frequency band associated with the alpha rhythm is also characteristic of another rhythm, the mu rhythm, which is visible in the central area of the cortex. The mu waves (8-13 Hz) and slow beta waves (13-15 Hz), are called Sensorimotor Rhythms (SMRs), as they are visible in the so-called sensorimotor cortices, i.e., posterior frontal and anterior parietal areas. It has been shown that SMRs undergo changes during motor behaviors, specifically these rhythms energy decreases before and during movement, or motor intention. This decrement is named Event-Related Desynchronization (ERD), and it is the decrease in rhythmic activity following an externally or internally provoked event, such as voluntary movement. ERD may be associated with a subsequent increase in SMRs immediately after movement, which is called Event-Related Synchronization (ERS) (Figure 1.14) [22].

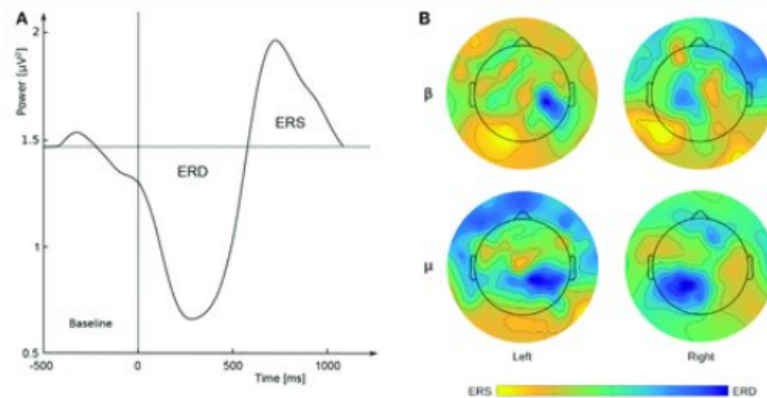


**Figure 1.14:** (A) Example of ERD/ERS time courses. (B) Maps of signal distribution on the scalp during motor imagery [23].

Both ERDs and ERSs are located in specific cortical areas and characterized by certain frequencies. These phenomena can be visualized in the time domain, by time-frequency analysis or with topographic maps. SMRs are due to a joint activity of cortical and subcortical regions, which are closely interconnected. Indeed, acquisitions performed with invasive electrodes revealed activity in the mu and beta bands in the thalamus, subthalamic nuclei, and pedunculopontine area [24].

The slow beta rhythm, as specified earlier, is characterized by frequencies ranging from 13 to 15 Hz and, like the mu rhythm, exhibits desynchronization in association

with motor behavior. The major difference between the two rhythms is that beta waves, in addition to ERD, develop ERS consequent to movement in the same brain area. This phenomenon is called beta rebound. The ERD and ERS associated with the beta rhythm, in fact, occur uniformly in the motor cortex, thalamus and subthalamic nuclei, while in the case of the mu rhythm, during movement, the ERD occurs in the motor cortex while the ERS associated with it occurs in the subthalamic nuclei. The beta rhythm (15-20 Hz) represents brain activation and conscious and intentional thinking. High beta waves (20-30 Hz) are typical of anxious states and agitation. Gamma waves are fast waves, with frequencies ranging from 35 to 45 Hz. These waves have very low amplitude and are found in moments of deep concentration [18].

### 1.2.3 Acquisition Electrodes

The system for measuring EEG signals is called an electroencephalograph. It consists of an acquisition system, that picks up the weak electrical signal on the scalp, a signal processing system, a storage and display system. The signal is acquired with surface electrodes, which are applied on the skin with the help of adhesive collars or patches, or are placed on a special elastic cap that fits over the patient's head. Because the outer surface of the scalp does not conduct sufficiently well, it is necessary to apply the electrodes with the help of a gel or electrolyte solution. This serves the dual purpose of promoting signal conduction, creating good electrode-to-skin contact, and maintaining adhesion between electrode and skin, reducing motion artifacts. Commercially available electrodes can be of different types, including cup electrodes made of tin and silver coated with silver chloride (Ag/AgCl), double-sided disposable Ag/AgCl electrodes, and stainless steel ring electrodes [25].

The most common acquisition method involves the use of the elastic electrode cap, with the electrodes placed on the scalp according to the arrangements defined by the 10-20 International Standard System. It consists of the placement of 21 electrodes on the scalp surface, located at intervals of the 10% and the 20% of reference lengths. The references are respectively the length of the skull in the transverse plane and the median plane, which are measured between two reference points, one placed at the base of the skull (inion) and the other at eye level, between the nose and forehead (nasion) (Figure 1.15) [26].

Depending on the experimental requirements, acquisitions can be carried out using two standard derivations, the monopolar derivation and the bipolar derivation (Figure 1.16). In the monopolar derivation, an electrode is placed at an active site and the reference electrode at an electrically neutral site. Reference sites generally are located at the mastoid, tip of the nose, earlobe or chin. This type of recording determines the absolute activity underlying the active site. In bipolar derivation,

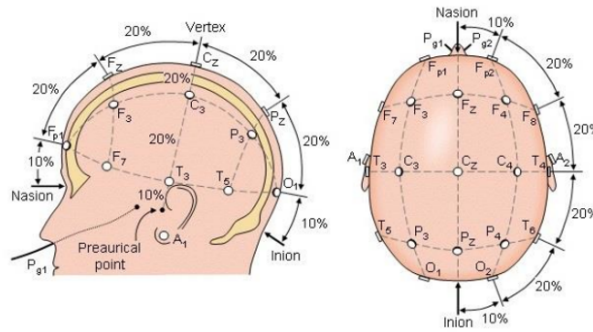


**Figure 1.15:** Electrode placement on the scalp according to 10-20 International Standard System [27].

both electrodes are placed on active sites in the area of interest, so the resulting signal corresponds to the difference between the signals recorded from the two sites [10].

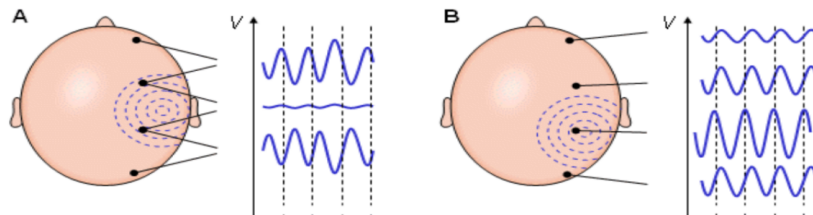


**Figure 1.16:** Example of monopolar and bipolar EEG derivations [28].

## 1.2.4 Acquisition Techniques

Surface EEG is a very low amplitude signal that reaches, in normal conditions, values of 50-100 microVolt. The recording system of such weak signals requires specific parameters in terms of signal amplification, noise rejection and electrodes impedance. Each channel is provided with a pre-amplifier, which must conform the following requirements:

- Differential gain of  $10^4$  order, which is achieved by two amplifier blocks arranged in cascade.
- Input impedance greater than 10 MOhm, which minimize the interconnection error that would otherwise further attenuate the EEG signal.
- High common mode rejection ratio (CMRR) to reduce the effect of interference due to ambient electrical noise, specifically interference due to 50 Hz power

lines. The CMRR defines the ability of a differential amplifier to attenuate the common-mode voltage while amplifying the differential mode voltage, and it is defined as:

$$CMRR = 20 \log \left| \frac{A_d}{A_{cm}} \right| \quad (1.2)$$

Where  $A_d$  is the differential gain and  $A_{cm}$  is the common-mode voltage.

- AC coupling of electrodes, which is achieved by placing a capacitor at the inlets of the pre-amplifier. AC coupling is used to remove continuous noise (DC) due to electrode potentials, which degrade the Signal to Noise Ratio at the output of the amplifier stage. The electrode potential depends on temperature and electrochemical composition and is much greater than the EEG potentials. If the electrodes were DC coupled with the pre-amplifier, the electrode potentials have to be perfectly equal to cancel their effect at the differential input of the amplifier. However, even using high quality electrodes of the same type, potential differences cannot be avoided, because the electrodes are placed at different locations on the scalp and their potentials are inevitably affected by variable parameters, such as temperature and electrolyte concentration of the gel. This potential difference generates a noise that is amplified and can drive the amplifier output into saturation. The presence of the coupling capacitor makes each entrance of the pre-amplifier to behave as a high-pass filter that attenuates the DC components.
- Isolation circuit, introduced to prevent the danger of micro- and macro-shocks.
- Amplifiers, which allow the required high gain to be achieved.
- Anti-aliasing low-pass filter, necessary to filter the signal so that it satisfies the assumptions of the sampling theorem. If the signal has to be sampled by Analog-to-Digital converter (ADC), its bandwidth has to be limited to satisfy Shannon's theorem, whereby, if  $f_s$  is the sampling frequency of the converter, the signal bandwidth must be contained within  $f_s/2$ , to avoid the distorting phenomenon of aliasing.
- Analog-to-digital converter, which has as input the sampling frequency  $f_s$  and the number of bits of the converter.
- Electrode impedance measurement circuit. If the impedance are too high, it increases the interconnection error and reduces the signal amplitude. In addition, unbalanced electrode impedance introduces differential noise that contributes to lower signal-to-noise ratio. Electrode impedance values below  $5 \text{ k}\Omega$  are recommended, with a maximum unbalance of  $1 \text{ k}\Omega$ .

The signal acquired in this way is then stored, processed and finally displayed on a monitor [13].

## 1.3 Brain Computer Interface (BCI)

The central nervous system (CNS) is responsible for processing external and internal information and stimuli and processing responses that are naturally muscular or hormonal. Brain Computer Interface is a system that record the CNS activity, extrapolate specific features and translates these features into artificial outputs that replace, restore or enhance the natural outputs of the body. BCI systems provide a direct communication channel that prescinds from the normal neuromuscular outputs of the CNS, enabling interactions with the surrounding environment for individuals with severe neuromuscular disorders. A generic BCI system consists of three parts: signal acquisition, signal processing and feedback, which is the tangible consequence of the subject's brain activity. Brain signals that serves as BCI's inputs can be recorded by a variety of different techniques, and carry different information depending on the recording method, in terms of frequency content, resolution, morphology and area of origin. The most common electrophysiological monitoring techniques use electric and magnetic fields in the brain, hemoglobin oxygenation values, and other signals recorded on the scalp or more invasive recordings within the brain. EEG is particularly suitable for applications with BCI because it is noninvasive, low cost, has wide spatial coverage and high temporal resolution. EEG-based BCI systems can be classified, according to the type of control signal used, into exogenous or endogenous, depending on whether or not the presence of an external stimulus is required to induce the manifestation of the signal. The most commonly used control signals in EEG-based BCIs are visual-evoked potentials (exogenous), P300 evoked potentials (exogenous), Slow Cortical Potentials (endogenous) and sensorimotor rhythms (endogenous) [6].

### 1.3.1 Motor Imagery driven BCI

Sensorimotor rhythms (SMR) are EEG signal fluctuations that can be detected over the motor cortex and correspond to alpha/mu rhythm (8-13 Hz) and beta rhythm (14-30 Hz). These rhythms are characterized by detectable energy modulations during motor tasks, either executed or imagined. These modulations occurring during motor execution, motor imagination or sensory stimulation are called event-related desynchronization (ERD) or event-related synchronization (ERS). ERD are defined by a decrease of the rhythms amplitude, while ERS correspond to an increase of the amplitude. The voluntary movement triggers the desynchronization of sensorimotor rhythms from about 2 seconds before the movement, in the controlateral hemisphere, and the same effect is originated by the motor imagery, as the immagination of movement engages the same cortical regions that activate during the actual execution [22]. Since SMRs consists of rhythmic oscillations, most BCIs developed starting from frequency analysis. The most common way to quantify sensorimotor

rhythms is to define the proportional power decrease (ERD) and power increase (ERS), by band-pass filtering each trial of the raw signal in a specific frequency band, squaring the samples and averaging over multiple trials [22]. A lot of other frequency-analysis techniques have been used to develop BCI systems, as the Fourier transform, the continuous wavelet transform, matching pursuit and autoregressive models. Alpha/mu and beta rhythms modulations are characterized by a somatotopic organization. The decrease of SMR that results from motor imagery or movement execution of different limbs is detectable in regions along the primary sensorimotor cortex corresponding to the interested body part, according to Homunculus organization of the cortex (Figure 1.17). This aspect of SMR offers a wider range of applications in the SMR-based BCIs field [29].

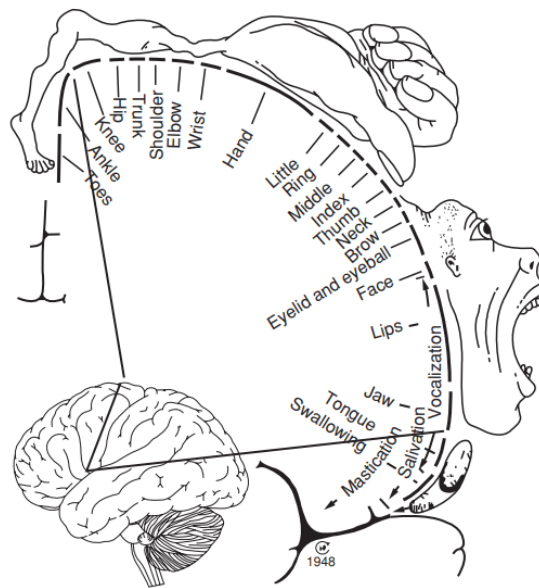


**Figure 1.17:** The motor Homunculus shows the effects of electrical stimulation of the cortex on human body parts [6].

### 1.3.2 FES-BCI System

Functional Electrical Stimulation (FES) is a technique that uses electric current to stimulate muscle contraction in order to generate functional movement. It provides a rehabilitative tool that can be used to help patients with persistent motor deficits to improve motor functions, by inducing an artificial muscular contraction. This treatment is effective only if the motor neurons of the target muscle are preserved, otherwise muscle activation cannot be triggered. FES system acts by approximately reproducing the neuronal stimulus, which under normal conditions triggers muscle

contraction through intact peripheral nerves. The current carried to the motor nerve is controlled by the electrical stimulator, which determines the pulse amplitude, frequency, duration, waveform and duty cycle. This current is delivered by means of electrodes, which are available as non-invasive surface electrodes or invasive implantable ones [30]. FES can be activated externally, by a predefined program or by a therapist. In these cases, however, the rehabilitation process turns out to be less effective than if the patient decides to activate FES by motor imagination effort. In fact, to stimulate muscle rehabilitation it is useful to enhance neuroplasticity, a phenomenon that occurs in the central nervous system and is responsible for altering its structure in response to internal and external stimuli, and this is achieved by promoting synchronization between the subject's intention and physiological feedback. FES used as a part of a brain-computer interface technology has been demonstrated to be a powerful tool to improve motor functions and facilitate the recovery of muscular activity, due to the ability of this system to promote neural organization and motor learning, as it provides proprioceptive sensory input along with an actual feedback, that is, visual perception of the movement. Real-time feedback of a BCI device provides an immediate reward-based reinforcement, that can be used to enhance the production of useful patterns of neural activity over others. This learned modulation, along with sensory input provided by FES, may promote the functional recovery of muscles and sensory pathways. BCI-FES systems synchronize the artificial movement with modulated brain activity, as the FES is activated only when appropriated brain signals events are detected during the imagination of the movement. This is the reason why this combined system has the potential to be more efficient than therapies that uses FES alone, as it focuses on neuromodulatory and neuroplastic motor learning aspects of rehabilitation.

## 1.4 Movement Intention Detection

### 1.4.1 Standard Approach

The standard approach to extrapolate features from physiological signals requires signal sampling, which is the conversion of the starting analog signal into a succession of samples. Samples are values taken from the analog signal at predetermined, equidistant instants. The time interval between two successive instants is called the sampling period, and its inverse the sampling rate. Sampling ensures the transition from the continuous set domain to the discrete domain. According to the sampling theorem (Shannon theorem), to avoid loss of information during the sampling phase of the signal, it is necessary to sample at a frequency greater than twice the bandwidth of the signal. The quantization of an analog signal is the process of discretization of the signal's amplitude. The sampled signal is divided into a finite set of intervals, and the samples in the same interval are associated with the

same output. As the sampling process, quantization results in an inevitable loss of information, which is quantified by the quantization error, which is the difference between the input value and the quantized value. The quality of the quantization process depends on the number of quantization levels; in particular, more are the levels, lower will be the associated error. The sampling rate and quantization error are parameters defined according to the desired specifications of the conversion system. ADCs used in EEG are characterized by sampling frequencies ranging from 256 Hz to 5 kHz. The resolution of the system is defined by the number of bits of the converter, which in commercial EEG has a value of 12 or 16 bits. The number of bits and the quantization number, which must meet the specification for the maximum quantization number of the system, allow the values to be mapped in a specific amplitude interval [13].

Once the signal is sampled, it can be analyzed with the help of different tools. The most common method used to extrapolate significant features from the EEG signal is the analysis in frequency domain with Fast Fourier Transform (FFT). This method allows an extensive examination of the discretized signal in terms of frequency characteristics, which are computed by Power Spectral Density (PSD) estimation. One method for PSD estimation is the Welch's method. The original signal is divided into  $M$  sections of equal length  $L$ , that can be overlapped:

$$x_i(n + iD), n = 0, 1, 2, \dots, M - 1; i = 0, 1, 2, \dots, L - 1; \quad (1.3)$$

Where  $iD$  is the starting point of the sequence.

A window is then applied to each section to produce the so-called modified periodograms.

$$P_{xx}(f) = \frac{1}{MU} \left| \sum_{\#n=0}^{M-1} x_i(n) \omega(n) e^{-j2\pi fn} \right|^2 \quad (1.4)$$

The parameter  $U$  is a normalization factor of the power, defined as:

$$U = \frac{1}{M} \sum_{\#n=0}^{M-1} \omega^2(n) \quad (1.5)$$

Where  $w(n)$  is the window function. The final Welch's power spectrum is achieved by averaging all the modified periodograms.

$$P_{xx}^W = \frac{1}{L} \sum_{\#i=0}^{L-1} P_{xx}(f) \quad (1.6)$$

Frequency domain analysis with Fourier is convenient because it allows the signal to be investigated as a sum of sine waves, thus allowing to isolate noise components from the useful signal more easily [31, 32]. EEG signal is non-stationary,

and this characteristic makes it theoretically unsuitable for analysis with FFT, which is a method applicable correctly only to deterministic signals or stationary or slowly varying stochastic processes. However, EEG signal can be assumed as stochastic and stationary if short intervals are considered. In order to execute an accurate analysis of locally stationary signals, it is important to consider that very short intervals bring to a more precise localization of discontinuities, but it makes more difficult a clean differentiation of frequency components. Time and frequency resolution depends on the definition of the length of the stationarity intervals and by improving one, the other deteriorates [33].

### 1.4.2 Energy-based Approach

The energy of the EEG signal is a parameter that allows the extrapolation of meaningful information regarding motion detection, or motion intention. One operator that allows to investigate the energy content of the signal is the Teager's energy operator (TEO). TEO is a nonlinear tool defined in both the continuous and discrete domains, that could continuously track the energy changes of the signal. This operation is largely applied to elaborate and analyze nonlinear modulation-type processes, as speech signals and audio signal processing. It has been used also to help the detection of the movement onset from the EMG signal [34] as this operator is characterized by a high sensitivity to instantaneous changes of the signal amplitude and subtle changes. This energy measure is derived from the product of the square of the amplitude and the square of the signal frequency. In fact, the total energy of a simple oscillating system, that is, the sum of kinetic and potential energies, is defined as [35]:

$$E = \frac{1}{2}mw^2A^2 \quad (1.7)$$

where  $m$  is the mass of the oscillating body,  $W$  is the frequency of oscillations and  $A$  is the amplitude. Teager's algorithm is developed using simple trigonometric hypothesis, starting from the signal of the motion of an oscillatory body, expressed as a periodic harmonic formula:

$$x_n = A\cos(\Omega n + \phi) \quad (1.8)$$

The essential harmonic energy that generate the signal can be then calculated as:

$$E_n = x_n^2 - x_{n+1}x_{n-1} = A^2\sin^2(\Omega) \approx A^2\Omega^2 \quad (1.9)$$

The Teager's operator is defined in the continuous domain as:

$$\Psi[x(n)] = \left(\frac{dx(t)}{dt}\right)^2 - x(t)\frac{d^2x(t)}{dt^2} \quad (1.10)$$

This function define the energy content of the signal and it depends only on the signal itself and its first two time derivatives. In discrete domain TEO is defined as:

$$\Psi[x(n)] = x_n^2 - x_{n+1}x_{n-1} \quad (1.11)$$

Where the operator is defined by three adjacent samples of the signal. Because of its properties, TEO could be involved in the developing of an event-driven technique to detect movement intention. The issue with the standard approach is that it is very consuming in terms of power, as it requires a constant sampling frequency and, consequently, the presence of the ADC in the hardware system. On the other hand, TEO enables an event-driven approach because it is a nonlinear operator implementable in continuous domain, hence it does not require the ADC to extract valuable informations from the signal. The major lack of this operator is that is very sensitive to noise. However, the effect of noise can be reduced by applying a proper filtering procedure to the signal. In particular for the application on EEG signal, it is important to pass the signal through band-pass linear filters, to minimize the error introduced by artifacts [36, 35, 37].

# Chapter 2

## State of the Art

### 2.1 FES-driven BCI Systems

The signal processing chain of non-invasive BCI-FES systems is defined by a specific sequential units. The first stage involves the acquisition of the EEG signal during motor imagery performed by subjects. The process of imagining motor activity causes oscillatory changes in sensorimotor rhythms. The next step is to provide a subject-specific calibration, and depending on the feature extraction model chosen, parameters can be defined for offline and online implementations. The detected motor imagery events are sent to the interface unit (feature translation), which activates the FES (device output). The FES delivers the stimulus to the patient as needed and thus the desired motion is achieved (Figure 2.1) [38].

Most commercially available BCI-FES systems are aimed at the rehabilitation of stroke patients. One of the first works for rehabilitation was done by Pfurtscheller et al., who implemented a system for restoration of hand grasp function using BCI-FES device in a quadriplegic patient. The patient was trained to generate changes in alpha and beta oscillations during motor imagination. The EEG signal during the MI task was acquired with 60 electrodes. The oscillations were band-pass filtered and Fisher's linear discriminant analysis was used for trial separation and classification. A threshold system was implemented to identify FES trigger events and subjects exhibited an accuracy of 83% in imagined movement. With this study, it was shown that in FES-driven BCI systems, the activity of EEG signals is strongly contaminated by FES-stimulated muscle activity, however, this activity is particularly visible in the lateralized EEG channel, but absent in the mid-central EEG recordings, which is the most relevant region for the detection of motor imagery-sensitive signals [39].

In another study conducted by McCrimmon et al. it was shown that BCI-controlled FES is an effective physiotherapy tool for lower-limb motor recovery in

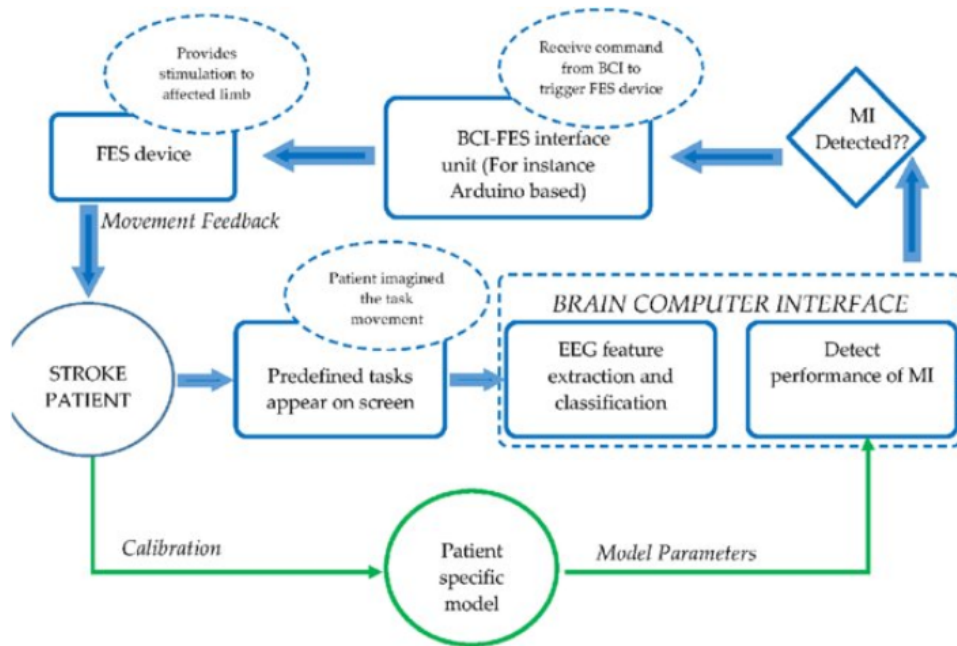


**Figure 2.1:** Schematic representation of BCI-FES system for neurorehabilitation [38].

stroke survivors, as it promote a lasting neurological and functional improvements. The main parameter used in this study was the Power Spectral Density (PSD) of the EEG signal recorded from a 63-channel system. The PSD was calculated for each trial in the offline calibration, it was then spatial filtered with class-wise principal component analysis (CPCA) to separate two different class of movements, then a linear discriminant analysis (LDA) was applied. The features were extracted from the signal and then classified using a Bayesian classifier [40].

Many studies focuses on the detection and recognition of different imagined movements, but that requires the involvement of elaborate spatial filters and machine learning analysis, which results in using a high number of electrodes and high computational power. The goal of this work was to develop a real-time implementable system that focuses on the detection of the hand movement using a single EEG electrode, by implementing also techniques of which the efficacy has been extensively tested, as the PSD. Another work that demonstrated the efficacy of a technique based on the PSD parameter for the detection of the movement was the one conducted by Aleksandra Vuckovic et al. [41]. In this work, bipolar derivation EEG recordings were used to calculate the PSD in the alpha and beta band frequency, and the subjects were able to control the suppression of the PSD during the motor imagination of an opening hand, thanks to the feedback provided

from a graphical user interface (GUI) (Figure 2.2). The hand involved (left or right) was chosen before the task as the placement of the electrodes was different depending on the imagery movement performed. FES was activated when the suppression of the PSD reached a predefined value. They demonstrated that once the FES was activated, even if the subjects stopped the motor imagery task, the movement stimulated by FES was able to keep active the motor-related areas of the brain, as the power suppression was still detectable. This system led to an accuracy rate of 83.5% for left hand and 83.8% for right hand.

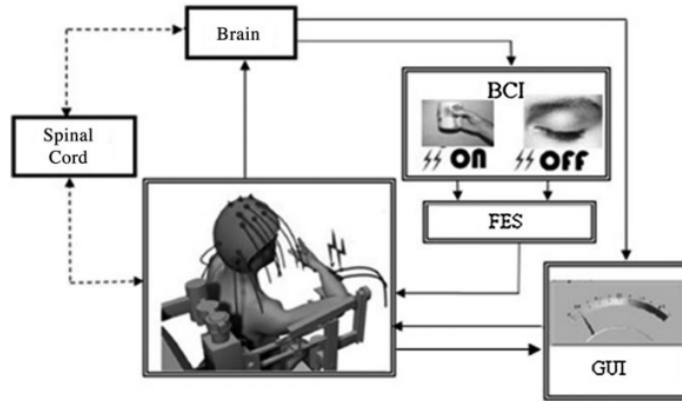


Figure 2.2: BCI-FES system developed in [41].

## 2.2 Single Channel EEG MI-based BCI Systems

Many studies have been conducted to detect motor intention from a single EEG channel. The use of a single channel often implies a signal corrupted by artifacts, which are normally minimized by using multiple channels, that allow the involvement of spatial filters for noise rejection. The presence of artifacts lowers the accuracy of the single-channel system ability to detect signal changes due to motor imagination. In [42] a single channel hybrid BCI system was developed. The system combined motor imagery (MI) related signals and steady-state visually evoked potential (SSVEP). For the recordings the subjects were asked to simultaneously perform an MI task and visually focus on SSVEP flicker. Feature extraction was performed with short-time Fourier transform (STFT) and common frequency pattern (CSP) method. To estimate the classification accuracy was used a linear discriminant classifier (LDC). This system achieved an offline accuracy of 85%, but it was not suitable for real time applications.

In [43] the motor intention detection from one channel EEG was achieved by using low frequency readiness potential (RP), a signal elicited in EEG during

imagery or real movement. RP is detectable in the delta bandwidth (0 – 5 Hz), but it is highly contaminated by low frequency transients artifacts. To minimize the transients, a total variation denoising (TVD) filter was applied. TVD is a nonlinear tool for efficient noise suppression that preserves at same time low frequency sharp edges and the shape of the signal underneath. The filtered signal was processed with Teager’s energy operator (TEO) and the events related to the movement were isolated by using a threshold and constraints related to morphological characteristics of the RP waveform. An accuracy of 91.2% was achieved in real movement execution tasks.

## 2.3 Wearable Systems

One of the goals of this thesis work was to define an accurate method for motor intention detection that can be employed in the development of wearable devices, suitable for real-time applications. There are a wide variety of noninvasive BCI devices on the market, characterized by a signal acquisition part and a translation part. The acquisition system contains electrodes, analog circuit and digital system for recording and signal transmission. The connection between the acquisition system and the translation part can be wired or wireless. The most famous companies producing wireless devices are G.tec, Emotiv, Open BCI, Neurosky. G.tec has marketed a wearable EEG device called G.Nautilus (Figure 2.3), which uses 32 analog-to-digital converters (ADCs) that enable very high sampling rates and high resolution.



**Figure 2.3:** g.NAUTILUS wearable EEG headset [44].

# Chapter 3

## Algorithms Description

### 3.1 Preliminary Assessments

Motor behavior generates changes in the EEG signals in the form of event-related desynchronization (ERD) and event-related synchronization (ERS). ERD is a localized decrease of the rhythmic activity amplitude in a specific frequency band. During imaginary or real movement, ERD of mu rhythms is visible in the central cortical area, as it is the result of an increasing excitability of central neurons. On the other hand, ERS represents an amplitude increase of cerebral rhythms. In particular, ERS results as beta rebound in the frequency band ranging from 15 to 30 Hz that occurs after limb movement. The analysis of ERD/ERS pattern in time and space during motor imagery is a valid indicator of the dynamics occurring in cortical networks [22].

In this work, ERD/ERS patterns were used to identify the specific frequency band in which motor imagery occurred (Figure 3.3). EEG signal changes related to motor behavior have been shown to occur primarily in the mu/alpha band; however, this band exhibits variability across subjects. Therefore, it is important to identify for each subject the precise range of frequencies in which motor activity is visible during the performed task [45]. The general method for calculating ERD is as follows (Figure 3.1):

- raw signal segmentation to obtain event-related trials;
- band-pass filtering;
- squaring of each trial samples to obtain power samples;
- averaging power samples across all trials to minimize the influence of artifacts and non related-event oscillations;
- smoothing the signal by averaging over time samples to reduce variability;

ERD is generally expressed as a percentage value, which is calculated as:

$$ERD/ERS(\%) = \frac{(E - R)}{R} * 100 \quad (3.1)$$

Where E is the event, identified as the signal in the period in which the motor imagery occurs, and R is a reference period prior to the event [46].

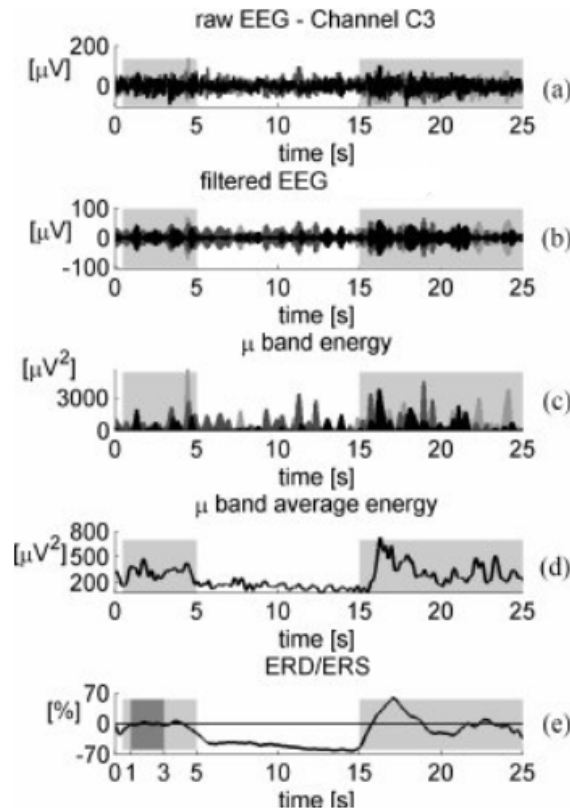


**Figure 3.1:** Example of ERD/ERS calculation method [46].

To determine the subject-specific frequency band, time-frequency analysis was performed on the signals, and the cerebral activity maps were plotted to identify the precise frequency range in which the brain activation occurred (Figure 3.3). Time-frequency analysis was executed using EEGLab, an open-source toolbox accessible from Matlab that allows an accurate processing and analysis of electrophysiological data. A baseline correction was applied to the signals and ERD/ERS calculation

was performed. ERD/ERS maps were created using a sinusoidal wavelet with minimum 3 wavelet cycles at lowest frequency and a coefficient of 0.8 for defining the number of wavelet cycles per data window at highest frequency. A p-value threshold of 0.05 was defined using the bootstrap method for defining statistically significant area and the False Discovery Rate method was implemented to correct the p-value across time and frequencies (Figure 3.2).



**Figure 3.2:** EEGLab Graphical User Interface to set the parameters to perform time-frequency analysis.

The aim of the developed algorithms is to detect the movement intention from one single EEG channel. Due to cerebral contralaterality, the signal developed by the imagination of the right hand is more pronounced in the left hemisphere. To detect the imagined movement of both the right and left hand, in preliminary tests only signals acquired from Cz channel were used, as it is placed over the cortical mid-line motor area and it is influenced by both the activity of the right and left hemisphere. However, this consideration is not valid for all subjects, as some subjects show enhanced activity for both imagined movements in a specific hemisphere. To ensure a better performance of this application, therefore, it is necessary to define during offline calibration a subject-specific placement of the single electrode, using time-frequency analysis to identify which area is most activated during motor imagination.

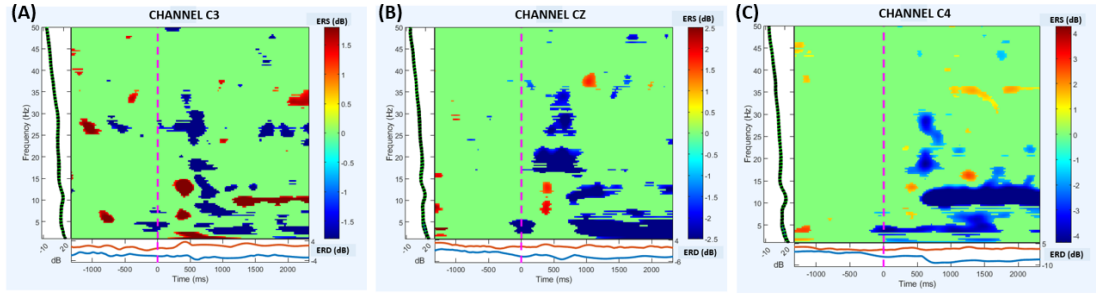


**Figure 3.3:** Time-frequency analysis performed on subject 1 during motor imagination task of both hands, second session. On the y-axis the power content of the signal in the frequency domain is shown. On the x-axis is shown ERD signal in blue and ERS signal in red. The onset of motor imagination is indicated by the dashed line. (A) The signal acquired from channel C3 shows minimal desynchronization (in blue) in the most active frequency band, followed by related synchronization (in red). (B) In Cz, intense activity is observed at low frequencies and slight desynchronization at the mu/alpha band. (C) In C4, a strong desynchronization is observed in the band of interest. This indicates greater brain activity during the task in the right hemisphere for subject 1. According to the time-frequency maps, the frequency range of greater activation for subject 1 is (9-14 Hz), and the channel that detects the major brain activity is C4. These two parameters will be used as input in the following processing.

## 3.2 Power Spectral Density (PSD) based Algorithm

### 3.2.1 Pre-processing

Motion intention is detected using the power spectral density (PSD) of the signal. This frequency-based parameter was chosen to analyse neuronal modulation of SMR because of its ease of application and straightforward interpretation. EEG signal is known to be susceptible to different sources of noise, so, to assess the actual effect of artifacts on data signal, independent component analysis (ICA) was performed. ICA is a widely used filtering technique for artifacts removal in EEG signal, however it is effective on signals recorded in multi-channel mode. This method consists of a linear decomposition of the original signal into linearly mixed independent components [47]. The signal recorded from electrodes placed all over the scalp is the weighted sum of many neural potentials, originated by different sources distributed on the scalp. ICA attempts to separate the highly correlated signals recorded from different locations on the scalp into subcomponents and

facilitate the recognition of artefact components, that can be subtracted from the original signal [48]. ICA application is not the most suitable method for the purpose of this work, as it requires signals recorded from a large number of electrodes to be considered effective, but it was tested on signals to evaluate how artifacts effectively change the algorithm performances. ICA was implemented in EEGLab toolbox, using signals recorded from 25 channels (Figure 3.4).

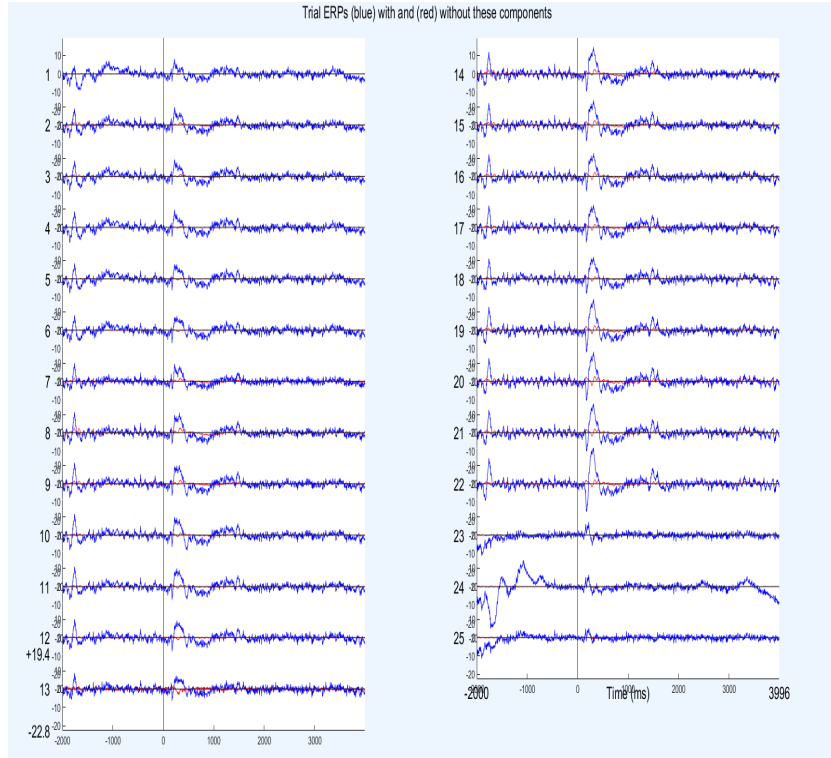


**Figure 3.4:** ICA analysis of signals acquired from 25 electrodes from subject 3 of the BCI competition IV dataset. The subject was instructed to perform a motor imagery task. The vertical line represents the onset of the task. In blue are the original signals, in red are the signals filtered with ICA. It can be observed that ICA effectively filters out artifacts.

After ICA application on signals, PSD was calculated. The analysis of Power Spectral Density of signals with and without artifact rejection leads to the conclusion that artifacts have small impact on the PSD in the frequency band of interest (Figure 3.5).

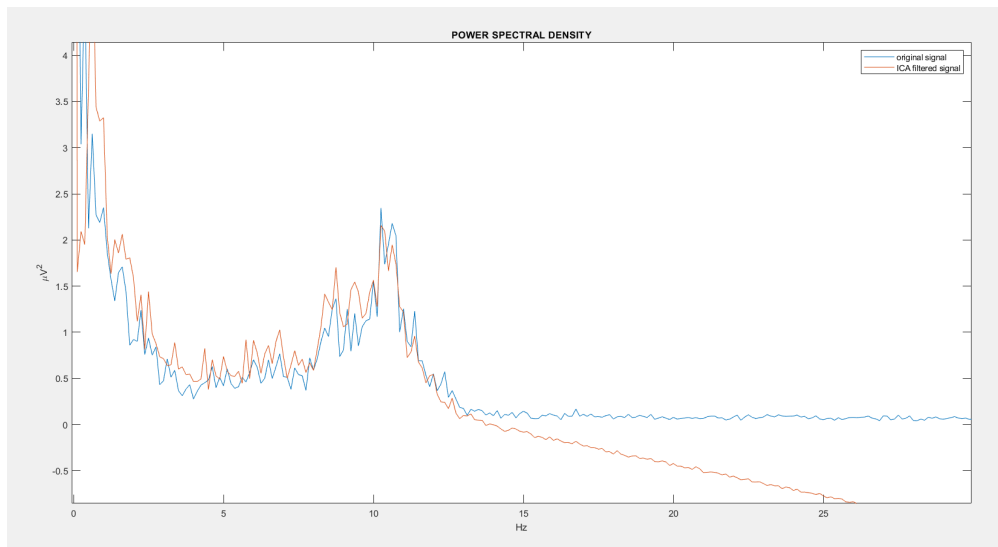


**Figure 3.5:** Power Spectral Density of Subject 3 EEG data. In blue the PSD of the non filtered data, in red the PSD of the ICA filtered data. The PSD on the mu/alpha range was not heavily affected by artifacts, indeed the filtering had a major effect on higher frequencies.

These results shown in Figure 3.5 have been confirmed by various studies, which show that the PSD technique is less susceptible to artifacts than other techniques [49]. Given the small noisy contribution of artifacts, to avoid higher computation complexity and power consumption, and to fulfill the single channel EEG request, artifact removal was not implemented.

### 3.2.2 Control Parameters

The PSD was calculated over a moving average window of 1 second to enable an online application and without overlap to maximize computation time. Different window lengths were tested and 1 second was defined as the optimal length according to performance results of the system. This interval length turned out to be the minimum time required for event-related power suppression to be recognized [41]. Within each window, PSD was estimated using non-parametric Welch's method, which is one of the most widely used approach for power evaluation in EEG processing studies [50]. PSD by Welch's method depends on three parameters:

- Window length and type
- Window overlap
- Number of FFT points (NFFT)

Hanning window type was chosen as it is characterized by a good frequency resolution and reduced spectral leakage. Window length was selected equal to 125 milliseconds. A small window size allows to obtain smoother PSD and to minimize the influence of noise, as it will be averaged out. However if the window length is chosen too short, it will compromise the frequency resolution, as the distance between two frequency points will rise (Figure 3.6) [51].

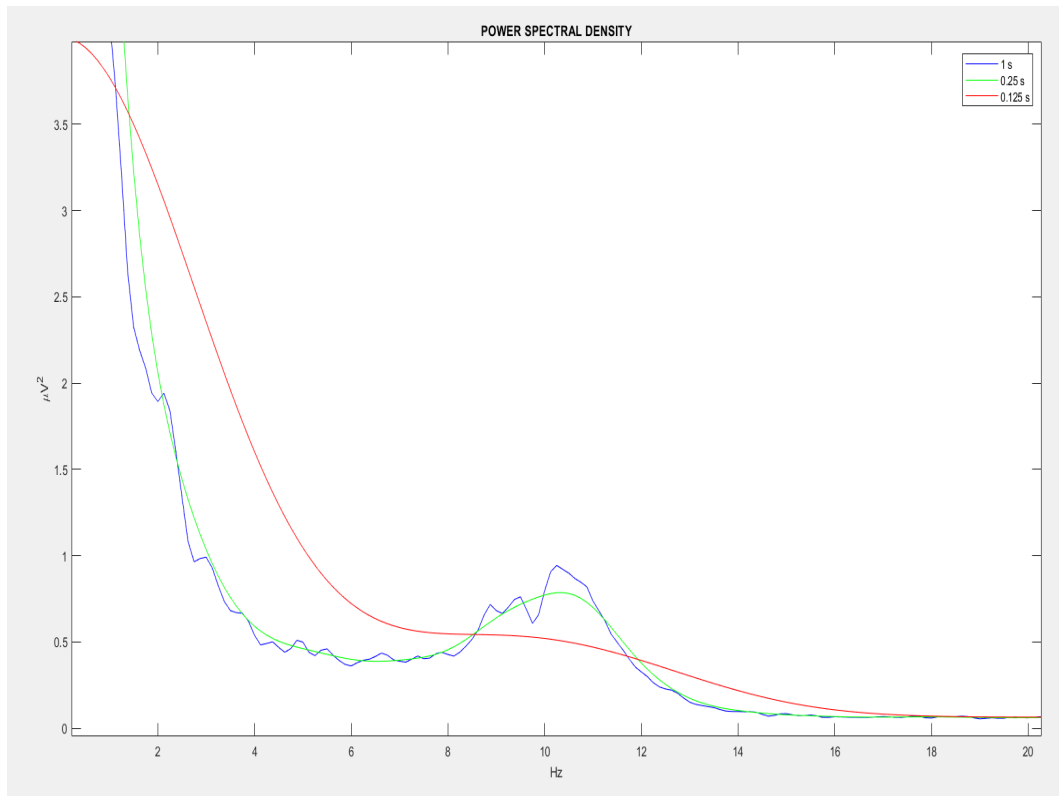


**Figure 3.6:** Power Spectral Density using Welch method for different window sizes.

A high overlap equal to 75% the window size was introduced to reduce the impact of noise. The number of FFT point defines the frequency resolution of the signal. Generally this number is set equal to the power of 2 of the window length. In this application, to obtain a resolution of 0.125, NFFT parameter was chosen equal to 2048. The PSD is defined in the frequency domain, so to obtain the signal power trend over time, the frequency band of interest was selected and the PSD signal samples within the predefined frequency range were summed. Each value obtained from the summation corresponds to a sample of the signal power in the chosen frequency band at a specific instant, as can be seen in Figure 3.7.

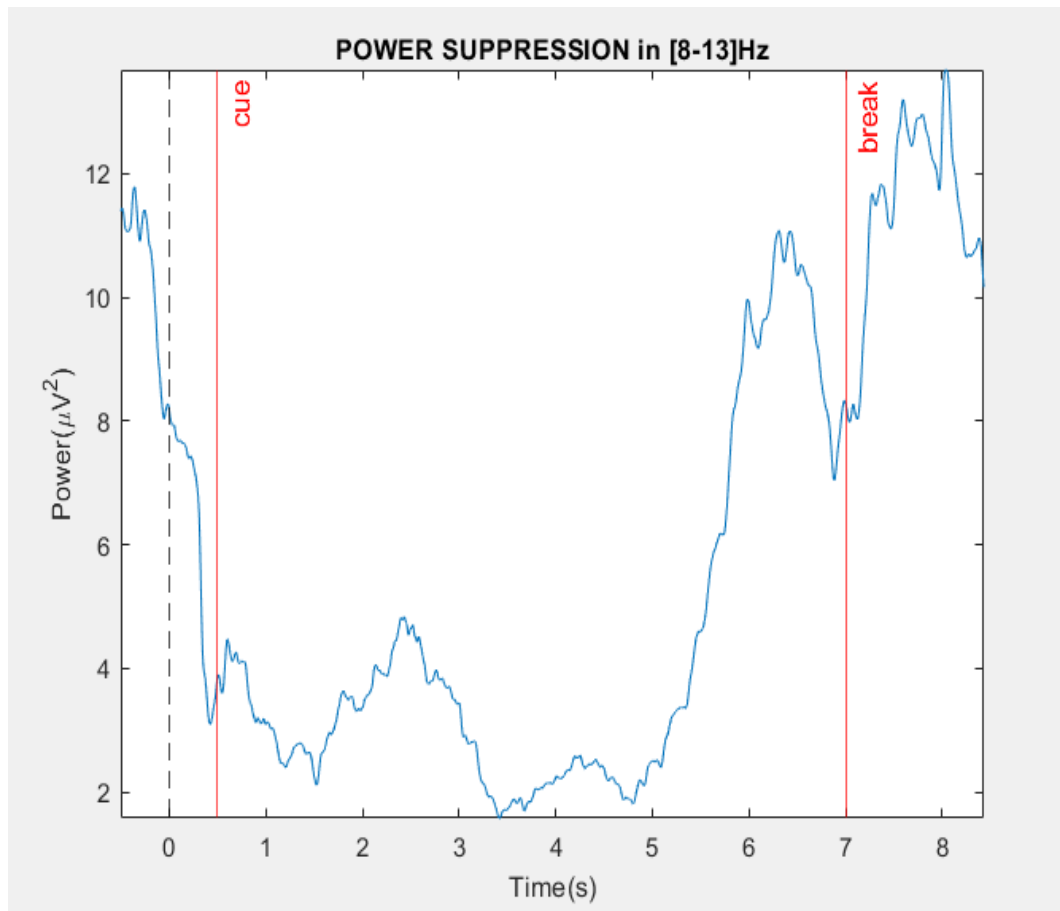


**Figure 3.7:** Plot of the power content of Subject 1 EEG signal in time domain during motor imagery. The suppression of the power can be seen after the motor imagery task onset.

### 3.2.3 Threshold Calibration

To detect the event generated by motor imagination, a threshold was defined with an iterative process (Figure 3.8). If the power signal calculated during an episode of motor imagination remained below the predefined threshold for an interval of 1 second, then it was submitted to a robustening process, in which the threshold was tested on a relaxation signal, recorded from subjects who were instructed to stay open-eyed without speaking. If the rest signal dropped below threshold for at least 1 second, then the threshold was increased and the iterative process was repeated, until a stable threshold was established (Figure 3.8).

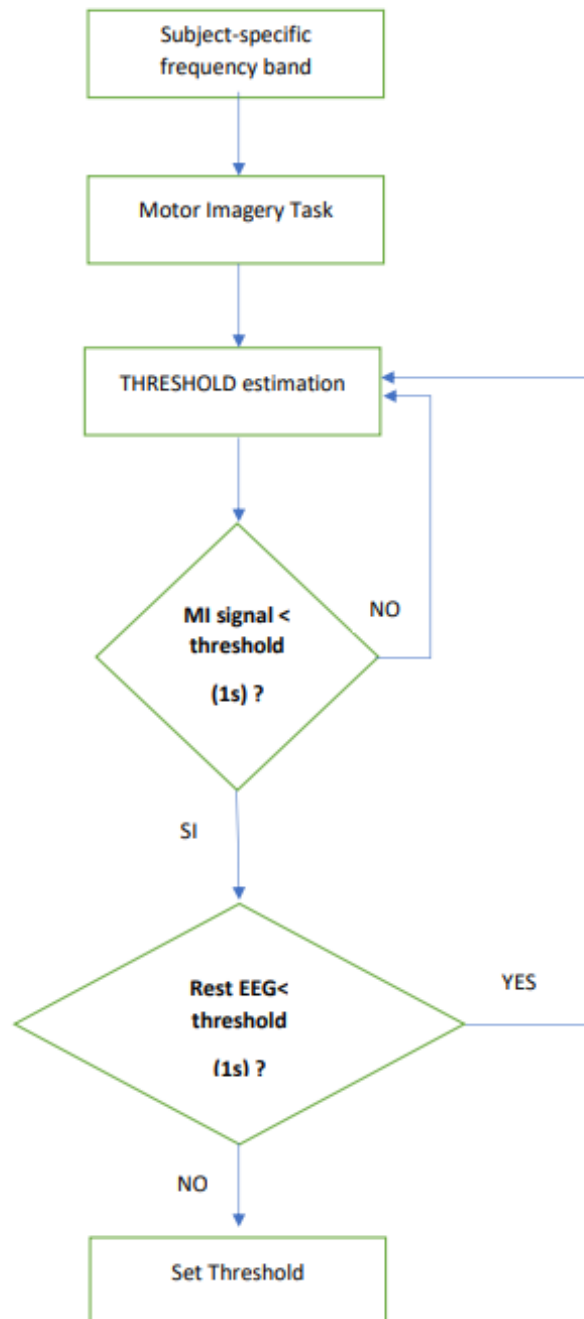


**Figure 3.8:** Iterative process to define a robust threshold for motor intention detection.

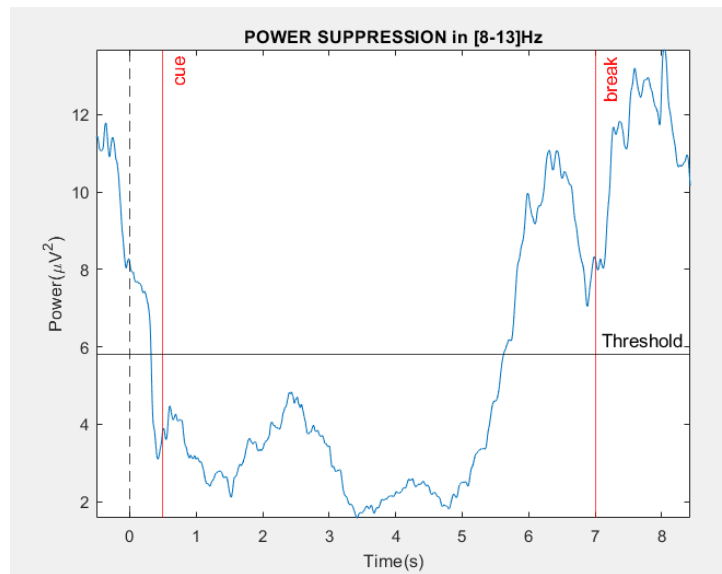


**Figure 3.9:** Time-controlled threshold.

The threshold was calculated during offline calibration for each trial, then the maximum threshold across each trial was selected. The power signal that remained below the threshold for at least the predefined time interval was identified as event.

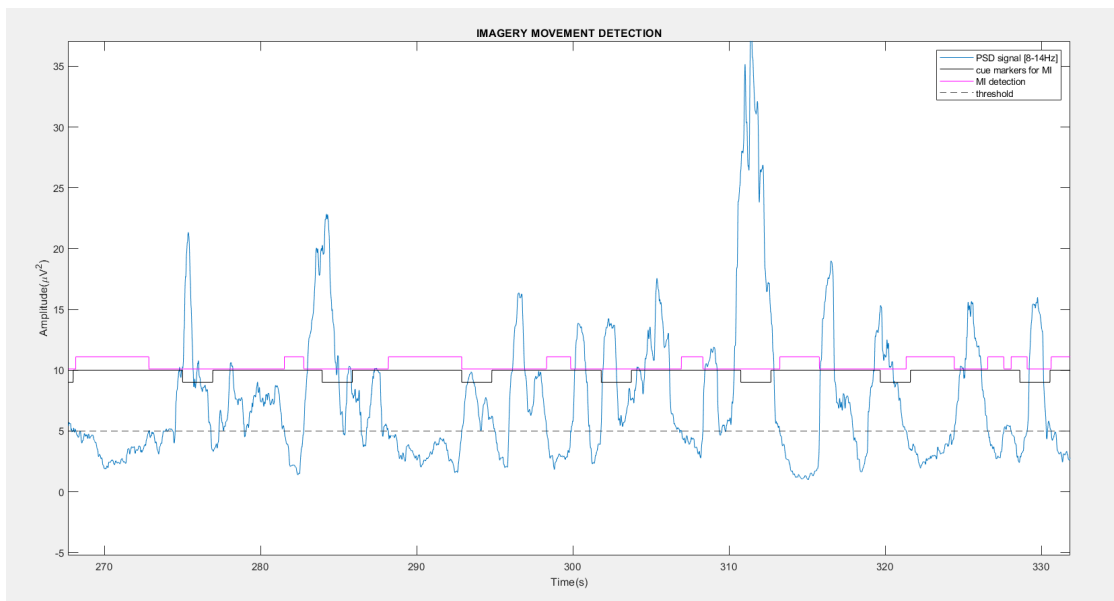


**Figure 3.10:** Subject 5 power content signal. The power of the EEG signal (in blue) had to remain below the threshold for at least 1 second after the task onset (in black) to be identified as an event (in magenta).

### 3.3 Teager-Kaiser Energy Operator (TEO) based Algorithm

#### 3.3.1 Preprocessing

The first step in the algorithm is to apply a filter to the original signal in order to isolate the band of frequencies of interest. As previously illustrated, the range of frequencies in which the signal undergoes changes during motor imagination is variable from subject to subject. Once the optimal frequency band is defined for each subject, the signal is bandpass filtered with a butterworth bandpass filter (Figure 3.11). The butterworth filter is widely used in electrophysiological signal processing because it has no passband and stopband ripple and has a shallow roll-off in the area where the roll-off is significant, that is, near the cutoff frequency [52]. This type of filter provides a linear response in comparison to others, which makes it the most suitable tool for separating the frequency components of the EEG signal and to minimize the influence of artifacts (Figure 3.12) [53].

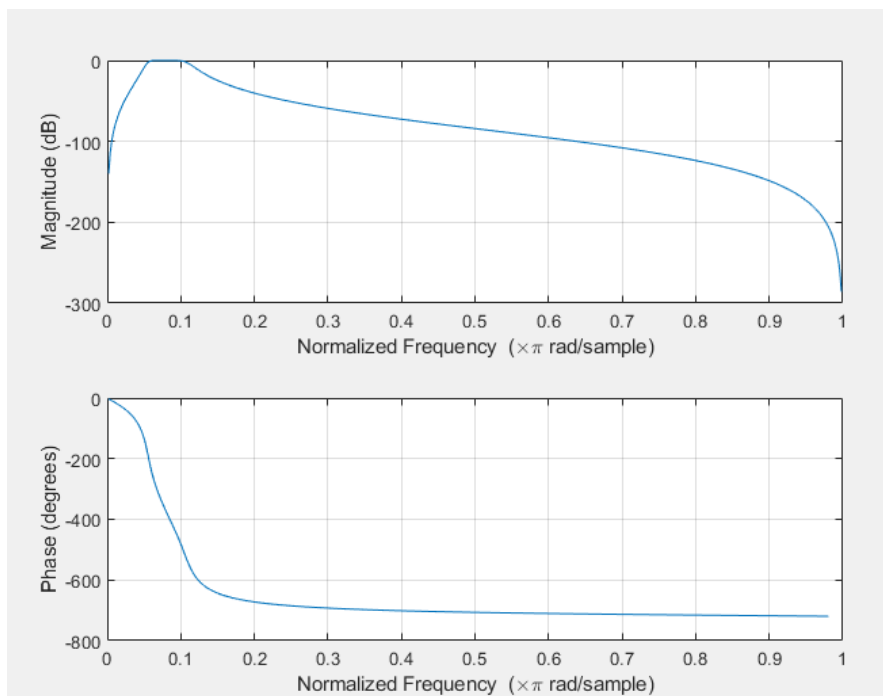
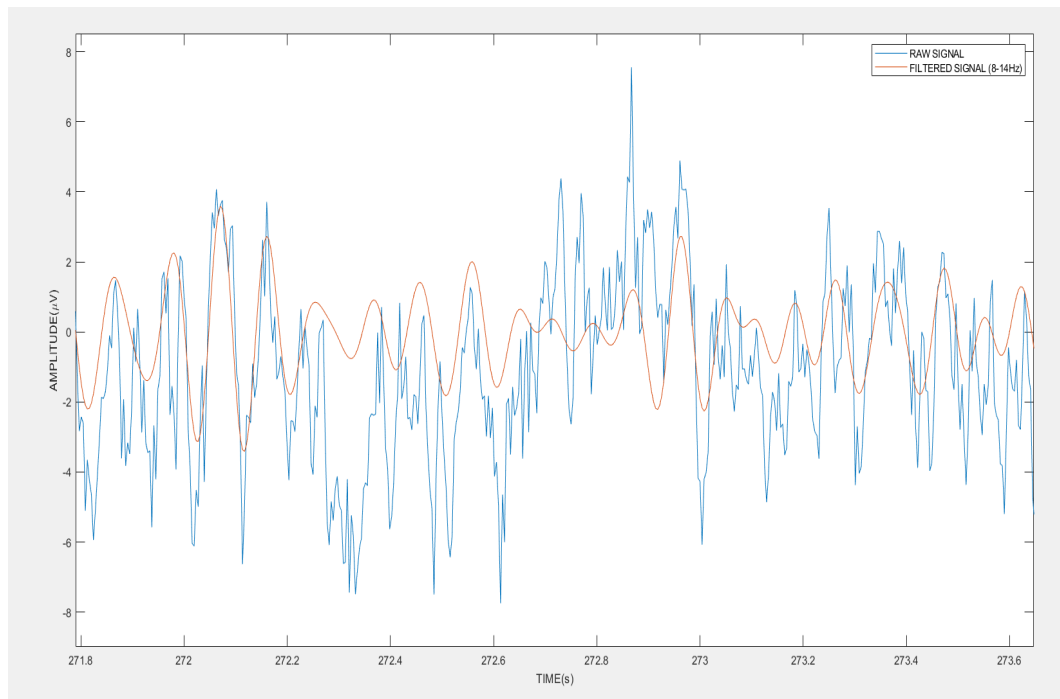


Figure 3.11: [8-14]Hz Bandpass Butterworth filter transfer function



**Figure 3.12:** Effect of the butterworth filter on the EEG signal.

EEG is strongly affected by artifacts, which contaminate the quality of the signal. The most common external noise sources, such as low-frequency transients or power line interference, are easily removed with simple high-pass and band-pass filters. Eye artifacts represent the most common physiological artifacts. They are generated by eye movements and blinks that propagate throughout the scalp due to the conduction volume phenomenon. These artifacts are characterized by an amplitude much larger than that of the EEG signal, and frequencies similar to those of the EEG signal. Although they are artifacts that propagate over the entire head surface, only the signals acquired from the frontal electrodes are severely corrupted by ocular noise. These artifacts are also present in signals acquired from electrodes placed in the central area of the scalp, but they are less influential [54]. The slight influence of EOG signal noise in the acquired signals was minimized during signal processing by imposing a limit on the amplitude of EEG signal oscillations, technique that will be explored later. Muscle artifacts can be caused by any muscle near the EEG signal recording site, and are due to facial micro-movements, swallowing, and jaw movements. However, the frequency distribution of muscle signals is outside the range of interest evaluated in this work. Cardiac artifacts originate from blood vessels near the acquisition site. The vessels dilate and contract, resulting in pulsating noise, which, however, is characterized by low frequencies, around 1.2 Hz, thus outside the band of interest [55].

### 3.3.2 TEO processed Signal

The second step is the application of Teager’s operator to the filtered signal (Figure 3.13). This operator is useful in the analysis of the EEG signal because it depends on its first two derivatives, so it has the characteristic of showing sudden changes in the signal such as discontinuities, frequency and amplitude variations, and it provides an accurate measure of signal energy over time [56]. The EEG signal in the selected band during a motor imagery task is susceptible to a phenomenon of desynchronization of neural potentials, resulting in a decrease in amplitude of the energy content of the signal, which is effectively detected by the TEO operator. The energy of the signal in traditional processing is calculated as the sum over time of the absolute value of the signal squared, or is estimated from the Fourier transform [57, 35, 58].

Teager and Kaiser, starting with a second-order differential equation, developed a new operator that can track changes in energy, starting with the observation that the energy to generate a simple sinusoid varies with frequency and amplitude. As illustrated previously, Teager’s non-linear operator is defined both in the continuous and in the discrete domain and potentially offers a simple and affordable tool to analyse the EEG signal.

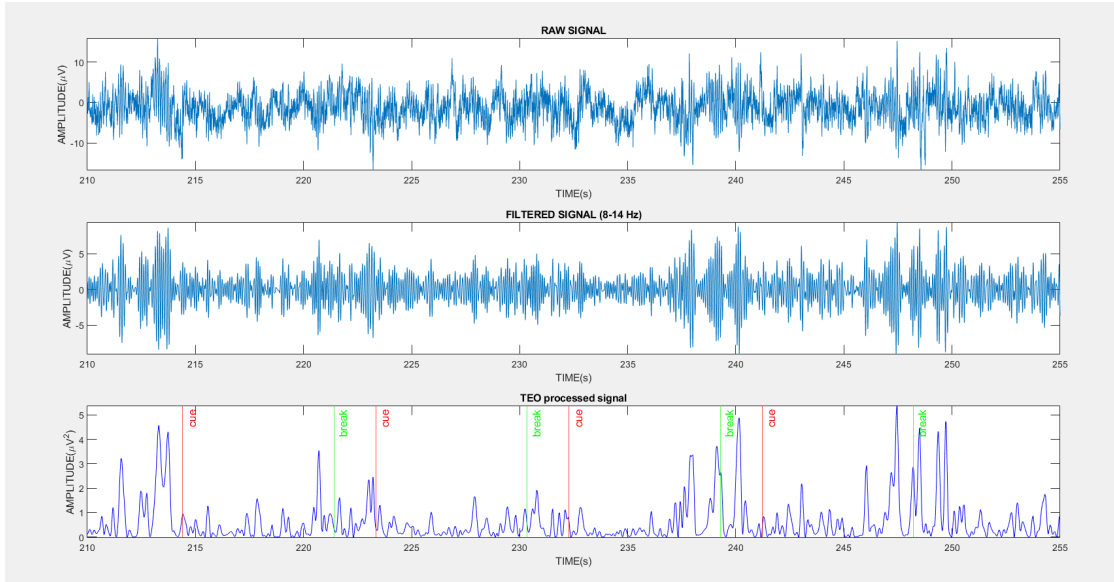


**Figure 3.13:** Preliminary steps of processing of the EEG signal of Subject 5 during motor imagery task.

### 3.3.3 Threshold and Amplitude Parameter Setting

Detection of the signal corresponding to motor intention, i.e., the event of interest, is accomplished using a threshold. The event is generated by the desynchronization of the action potentials of neurons involved in processing motor activity; this results in the decrease in the energy content of the original signal. Event recognition occurs when the TEO signal remains below the threshold for a predefined time interval. The time interval was chosen based on the characteristics of neuronal desynchronization, and in order to recognize the energy decrease as an actual response of an activity related to motor imagination, an interval of at least 300 ms was established. Desynchronization lasts from a few hundred milliseconds to a few seconds, but in order to develop a real-time system, capable of detecting the event quickly, the length of the minimum interval within which energy decrement can be defined as an event was chosen. The threshold was defined as follows:

$$Threshold = mean(TEO_x) + k * \delta(TEO_x) \quad (3.2)$$

Where  $\delta$  is the standard deviation of the signal. The value of the coefficient  $k$  was defined using a Receiver Operating Characteristic (ROC) curve, to optimize the performance of the system (Figure 3.14).

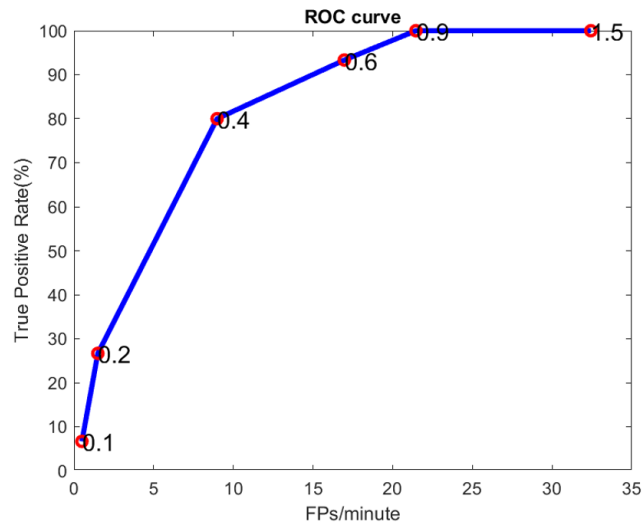


**Figure 3.14:** ROC curve of Subject 5 to determine the optimum value of  $k$  coefficient. The curve was obtained by changing the  $k$  value and evaluate the consequent response of the algorithm. The appropriate  $k$  coefficient in this case was chosen equal to 0.4, as it led to a good accuracy without causing an excessive increase of FPs/min number.

Each value of  $k$  was tested as a function of the number of True Positive Rates (TPRs) and False Negatives per minute (FPs/min). The  $k$  value chosen was the one that guarantees the highest number of TPRs versus the lowest number of FPs/min. If the signal remains below the threshold for a minimum duration of 300 ms, then the binary output corresponding to that interval was set equal to 1, otherwise it was set equal to 0. The binary output represented the activation signal of the subject's motor imagination.

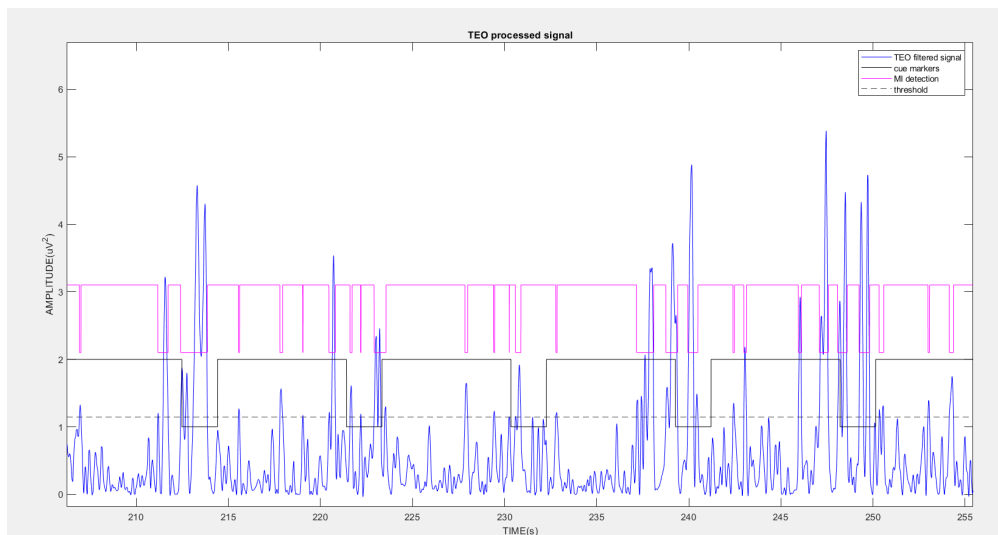


**Figure 3.15:** TEO signal of Subject 5. In magenta, the events detected by the first threshold block.

As can be seen in Figure 3.15, this first detection block provides an approximate tool for event detection; however, it is not sufficiently accurate by itself, because it cannot always discriminate the energy deflection representing the event and the random noisy oscillations. The TEO operator is extremely sensitive to the background noise of the EEG signal. Noise generated by ocular artifacts, transients, and random fluctuations that corrupt the EEG signal affect the operator's performance. The effects of these perturbations become significant because they are amplified by the squaring operations employed to estimate the necessary parameters by the Teager's operator, who can detect signal changes due to motor activity but lacks the ability to discriminate these signals from noisy perturbations [59].

To clean the output signal and accurately classify the event of interest, morphological considerations were made on the signal. Energetically, the signal exhibits homogeneous deflection during the activity of imagining or performing the movement [60], so to discriminate the signal from noise, it is useful to observe the presence of rapid oscillations with high peak-to-peak amplitudes (Figure 3.16).

These oscillations are in fact the result of the TEO operator's processing of the noisy perturbation, which in the original EEG signal manifests as a discontinuity and is energetically translated as a sudden increase in the TEO signal.

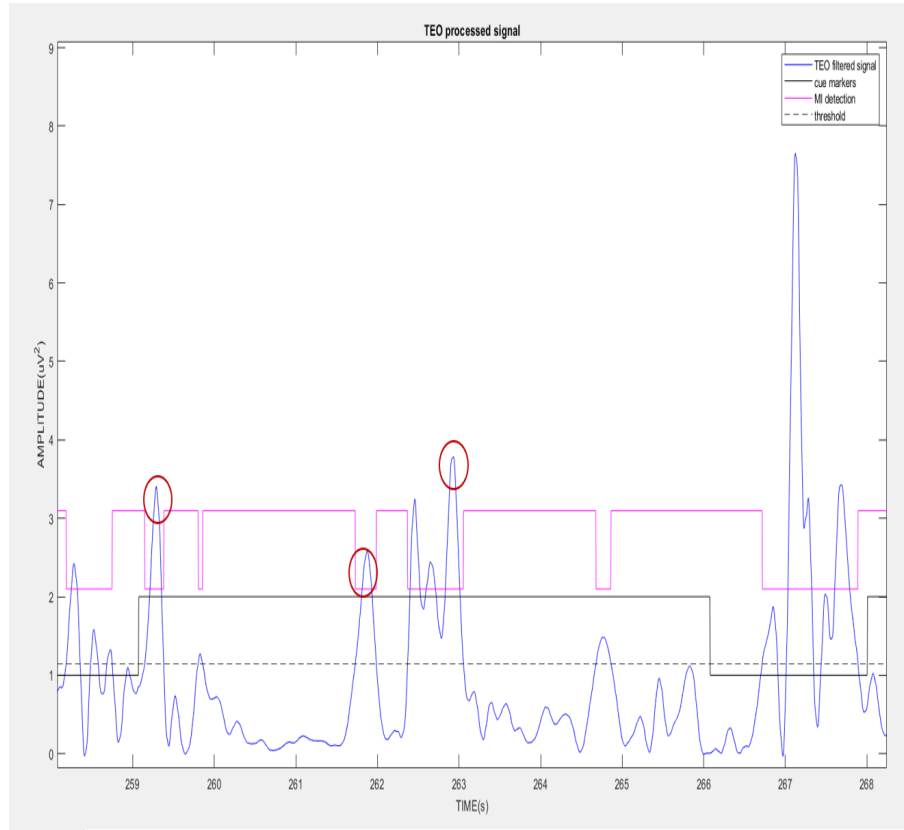


**Figure 3.16:** Example of high peak-to-peak amplitude noisy oscillations in Subject 5 TEO signal.

A second block that takes as input the segments of 300 ms duration, previously processed by the threshold method, was introduced, to minimize the influence of noise by identifying peaks with excessively high amplitude. If there were found oscillations in the considered window that were recognized as noise, the binary output at that window was set to 0, otherwise it was set equal to 1. The amplitude constraint of the noisy oscillations is defined by means of an ROC curve (Figure 3.19), which, as in the evaluation of the threshold parameter  $k$ , is useful in understanding how system performance varies depending on the amplitude coefficient chosen. Thus, the parameter chosen depends on True Positive Rate and the number of False Positives per minute.

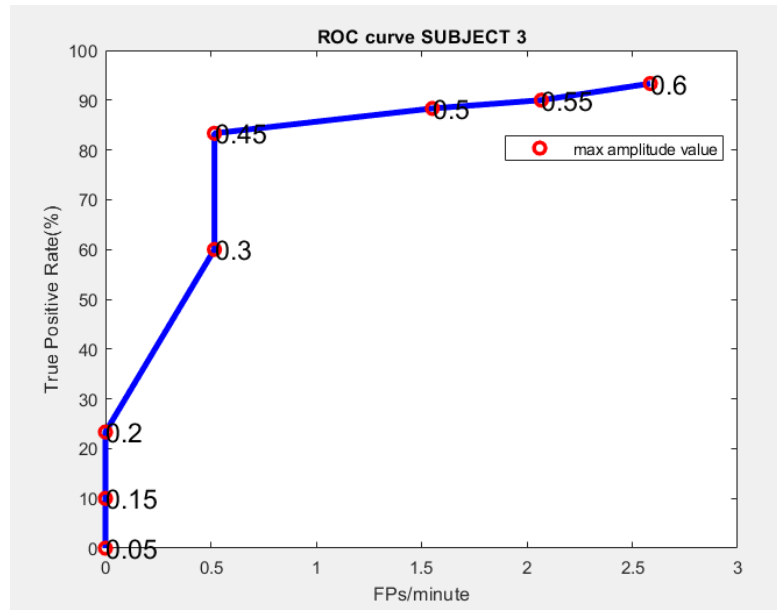


**Figure 3.17:** ROC curve for determining the maximum peak-to-peak amplitude of noisy oscillations.

As can be seen in Figure 3.18, the application of a second block to minimize the noise is significant in improving the accuracy of the algorithm, which shows improved ability to recognize motor imagination events and reject false positives.

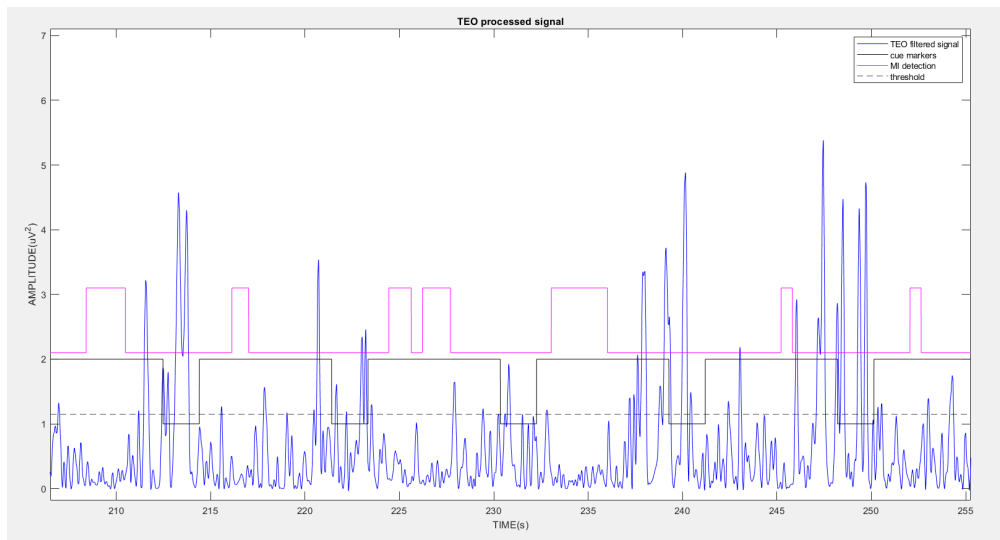


**Figure 3.18:** Subject 5 TEO signal

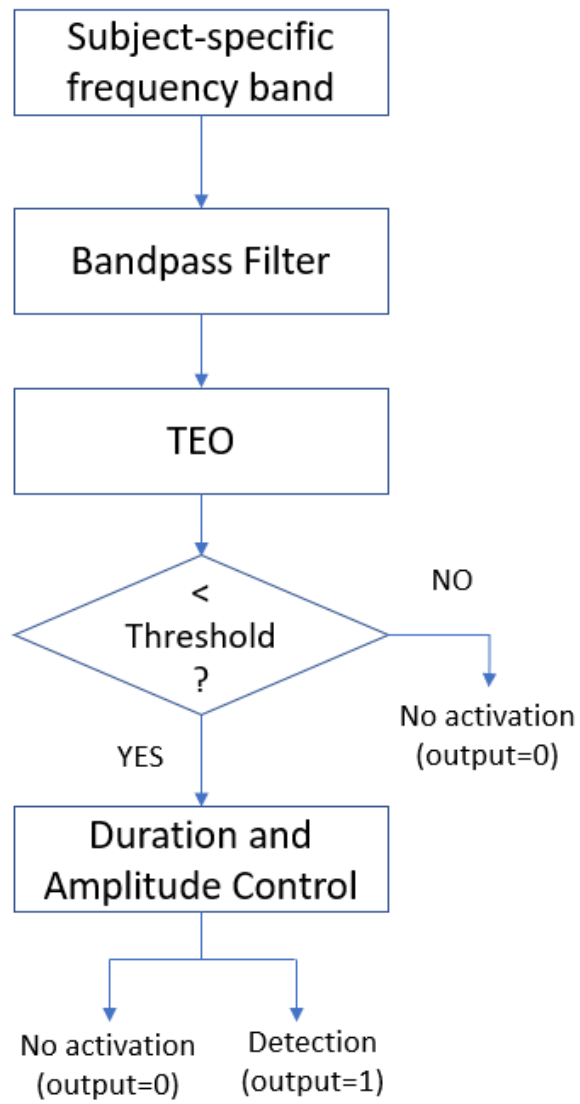


**Figure 3.19:** Steps of the TEO-based algorithm for motor intention detection.

# Chapter 4

## Intervention Protocol Description

### 4.1 Experimental Set-Up

Experimental acquisitions were made with g.tec HIamp, a tool used for measuring, processing, recording and reviewing biosignal data. Five subjects participated in the experiment. All subjects were volunteers, male, aged between 24 and 26 years. EEG signals were collected using Ag/AgCl active electrodes, placed on the proper elastic cap, that was available in the g.tec kit. The electrodes montage was based on 10-20 international system (Figure 4.1). Different electrode configurations were tested in order to identify the best arrangement for the desired application. In general, 12 electrodes were always used for EEG signal recording: Cz, C3, C4, CP3, FC3, CP4, FC4, O1, O2, T7, T8, plus a reference electrode placed on the left ear. The electrode placement was defined to cover the central cortical area of both cerebral hemispheres (Figure 4.2). The greatest neuronal activity during motor imagery tasks occurs in areas covered by electrodes Cz, C3 and C4, but the signal propagates on the scalp because of the volume conduction, so in addition to simple monopolar acquisitions from these three electrodes, bipolar acquisitions were recorded too, to examine how the signal changes from one site to another and from one derivation to another.

G.recorder, the software provided from g.tec for the acquisition and the visualization of the signal, enables the selection of the desired derivation, monopolar or bipolar. The bipolar configurations tested were performed from C3 and C4 channels, using Cz as EEG ground, and another configuration was CP3-FC3 and CP4-FC4. The recordings had a dynamic range of  $\pm 100 \mu\text{V}$  and a sampling rate of 256 Hz. The immediate preprocessing performed through g.recorder was a bandpass filtering of the signal between 0.1 Hz and 100 Hz. This preliminar filter

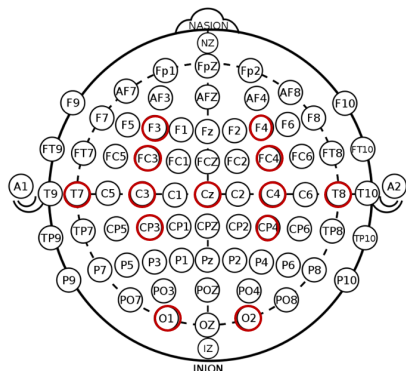


**Figure 4.1:** International System 10-20. Electrodes highlighted are the ones employed in the acquisitions.



**Figure 4.2:** Electrode's placement on Subject 2 during on-site recording.

allows to eliminate the low frequency noisy transients and to limit the frequency band, as the EEG signal does not have frequency components higher than 100 Hz. It was applied also a notch filter to minimize the power line noise, defined in a frequency range of 48-52 Hz. Subjects were comfortably sitting in an armchair, watching a screen monitor located in front of them. Each subject was instructed to perform two sessions of motor imagery tasks, one session of real movement execution and a final rest signal acquisition was performed (Figure 4.3).



**Figure 4.3:** Experimental set-up.

## 4.2 Cue-Based Motor Imagery Task

To record the motor imagery related signal was used a cue-based paradigm (Figure 4.5). Each subject was instructed to sit in front of a screen and perform a task based on what appeared on the screen. The paradigm consisted of two classes of imagery, left and right hand motion imagery. Each session of motor imagery consisted of 30 trials for each type of movement, for a total number of 60 trials. Between each session, a maximum of 10 minutes break was given. Before performing the first motor imagery task, the subject was instructed to perform a session of real movement. This session of movement execution was used to help the subjects to imagine better the movements in the following tasks, but also to verify that the system was working correctly and that the motor activity was detectable from the EEG signal. A signal consisting of 60 s of rest state was recorded, and the subject was simply instructed to remain relaxed, without talking or moving, but free to move the eyes and blink. Each trial started with a fixation cross and, 500 ms later, an arrow pointing either the left or the right, in a random order, was presented for 7 seconds. Over this period, the subject was instructed to imagine the corresponding hand movement. Each trial was followed by a break of at least 2 seconds, in which the blank screen re-appeared. A randomized time of up to 1 second was added to avoid adaptation (Figure 4.4).

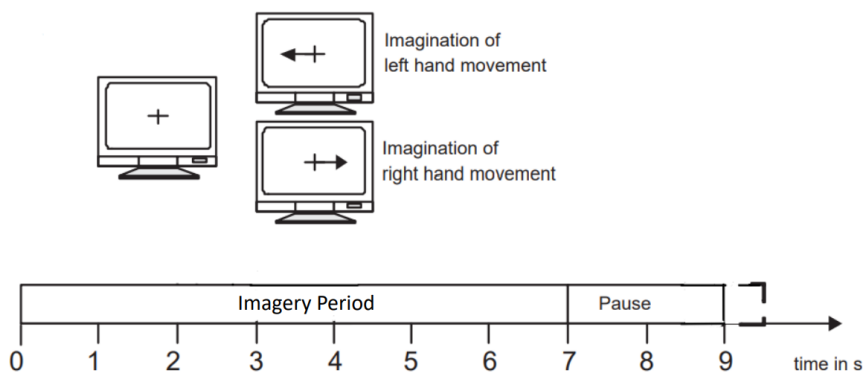


**Figure 4.4:** Timing scheme of the paradigm.

The session of real movement execution was conducted using the same paradigm. The real movement signals were not used in the development of the algorithms, they were acquired with the aim to provide a short training to the subjects and to assess the functioning of the system and paradigm.



**Figure 4.5:** Subject was instructed to watch the instruction on the screen and perform motor imagery till the cue disappeared.

## Chapter 5

# Experimental Results and Discussion

### 5.1 Quantification Parameters

The system performance was evaluated over an offline calibration and a simulated online session. The offline calibration was performed on the first session recorded, consisting of 30 trials in which left or right hand motor imagery was executed. This step allowed the definition of subject-specific parameters (frequency band, channel of major activity, threshold, window length, amplitude coefficient). These parameters were tested over the second session recorded. The simulated online test was performed using a while loop in Matlab version 2021, that took as input one signal sample at a time, to replicate the continuous data acquisition implemented by a real-time system. The loop was interrupted and the event was counted when the signal was found below the threshold for a predefined time interval. To provide a complete view of the performances of the two implemented methods, matrix based metrics were employed (Table 5.2), in which True Positive (TP), False Negative (FN), False Positive (FP) and True Negative (TN) values were reported.

The calculation of these parameters was based on the following assumptions:

- Subjects were required to follow the instructions appearing on the screen. The assumption is that subjects had the ability to start the motor imagery when the cue was presented on the screen.
- It is assumed that subjects could stop the motor imagery when the cue disappeared and the blank screen was presented.
- Subjects was instructed to focus on imaging doing the movement, rather than simply visualizing it. The ability to re-creating the feeling of the movement is

called Kinesthetic Imagery (KI) and it is different from Visual Imagery (VI). VI results in weaker SMR deflections, that could bring to a mis-classification if the signal is not low enough to remain below the threshold. On the other hand, KI translates in greater brain activity in the central cortical region and results in a simplest recognition of the event [41].

		PREDICTED VALUES	
		POSITIVE	NEGATIVE
ACTUAL VALUES	POSITIVE	53	7
	NEGATIVE	8	52

**Figure 5.1:** Confusion Matrix (CM) presenting TP, FN, FP, TN values of TEO-based algorithm tested on Subject 1.

		PREDICTED VALUES	
		POSITIVE	NEGATIVE
ACTUAL VALUES	POSITIVE	0,88	0,12
	NEGATIVE	0,13	0,87

**Figure 5.2:** Normalized Confusion Matrix (NCM) presents the results in a more intuitive way, but the information related to the dataset (i.e. number of trials) is lost during normalization.

True Positive is the outcome when the system identifies the event while the cue is presented on the screen (Figure 5.3). Following the suppositions made previously, in particular assuming that the subjects imagined the movement when the trial started, for each trial, a TP is counted only at the first activation during cue presentation, if the activation occurs, and that constitutes the output event (Figure 5.4).

False Positive is the outcome when the system incorrectly identifies an event in the period of time in which the blank screen is presented. Each event incorrectly recognized was counted as FP (Figure 5.6).

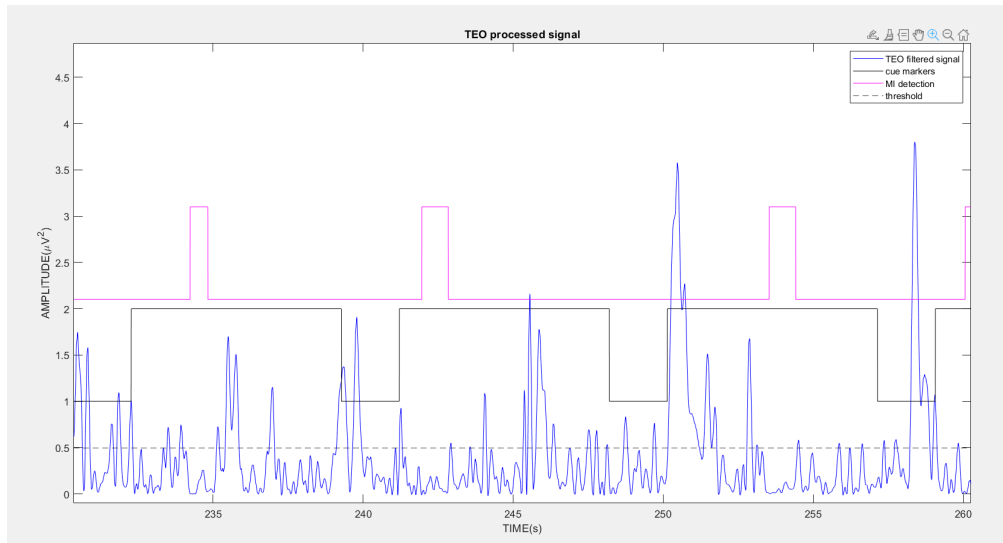


**Figure 5.3:** Example of TP detection from TEO-based signal of Subject 1. TP are defined when the system identifies the event after the onset of the task, while the cue is presented on the screen.

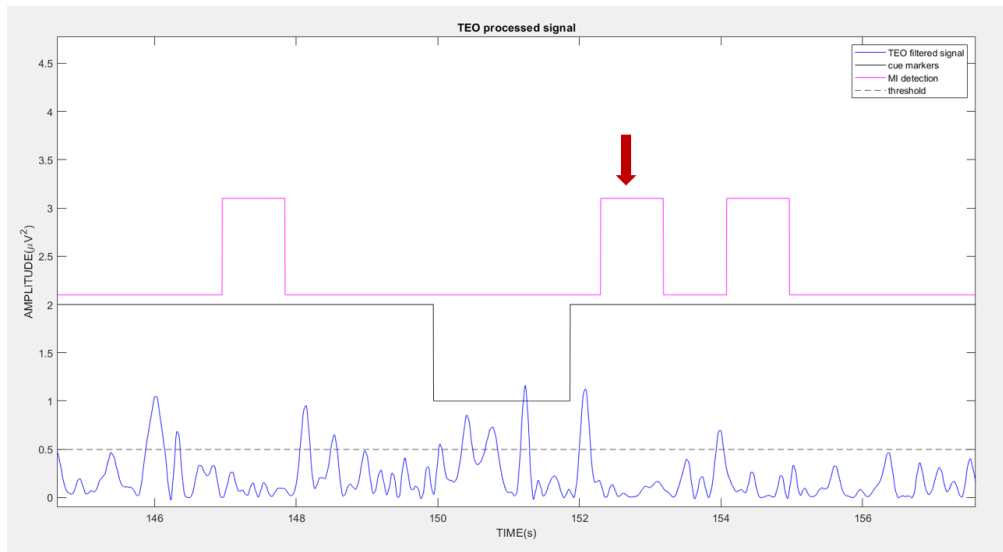


**Figure 5.4:** Example of TP detection from TEO-based signal of Subject 1. Even if two or more events are recognized, TP is counted only at the first activation during cue presentation.

In case an event was identified prior the onset of motor imagery, and continue during the time interval aimed at motor imagery, the event was not counted as FP (Figure 5.7). This consideration was done according to numerous studies ([61, 62,

63, 64, 65]), which showed that when the subject is mentally ready to perform or imagine an action, then brain activity prior to the onset of movement developed in preparation for the movement itself.

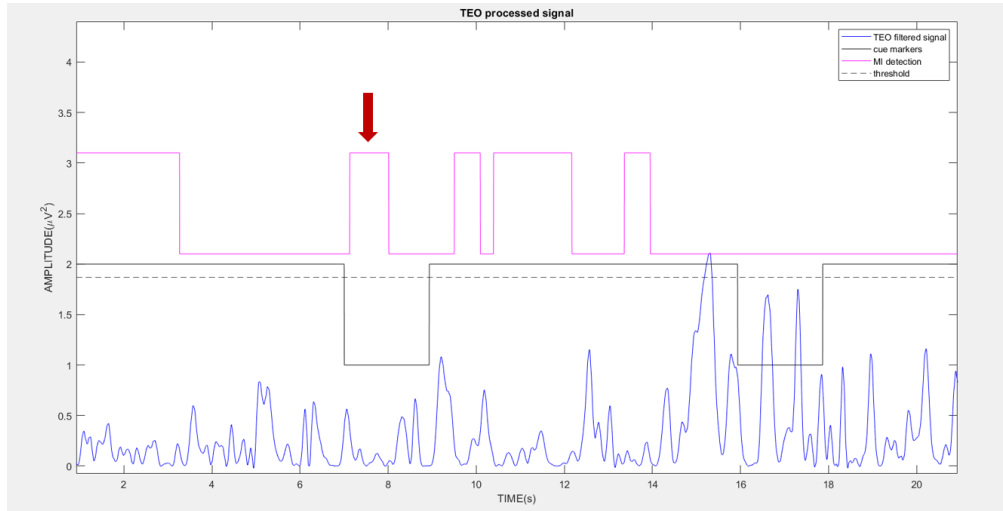


**Figure 5.5:** Example of FP detection from TEO-based signal of Subject 2. FP is counted when the algorithm identifies an event in the period of time in which the blank screen is presented.

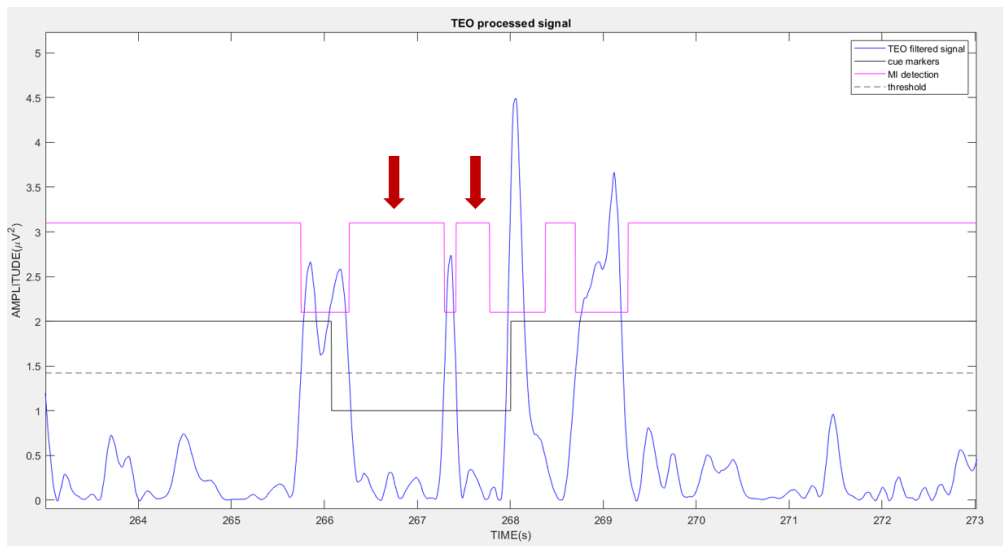


**Figure 5.6:** Example of FP detection from TEO-based signal of Subject 2. If two or more events are recognized during the rest period, all these events are counted as FP.

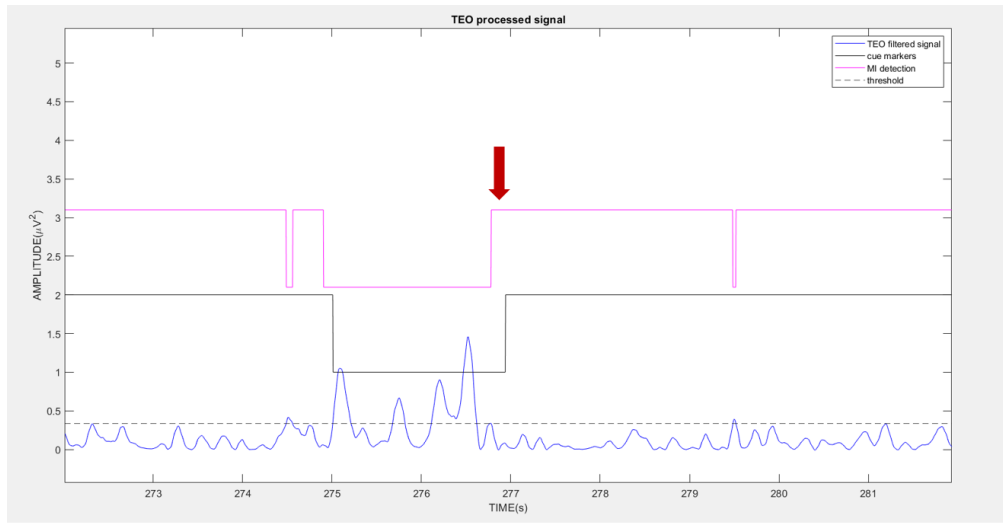


**Figure 5.7:** Example of FP detection from TEO-based signal of Subject 1. If the event (pointed by the arrow) was identified prior the onset of motor imagery, and continue during the time interval aimed at motor imagery, the event was not counted as FP

False Negative is the outcome when the model does not recognize an event during the motor imagery time interval, while True Negative results when the system does not identify an event when the blank screen is on (Figure 5.8).

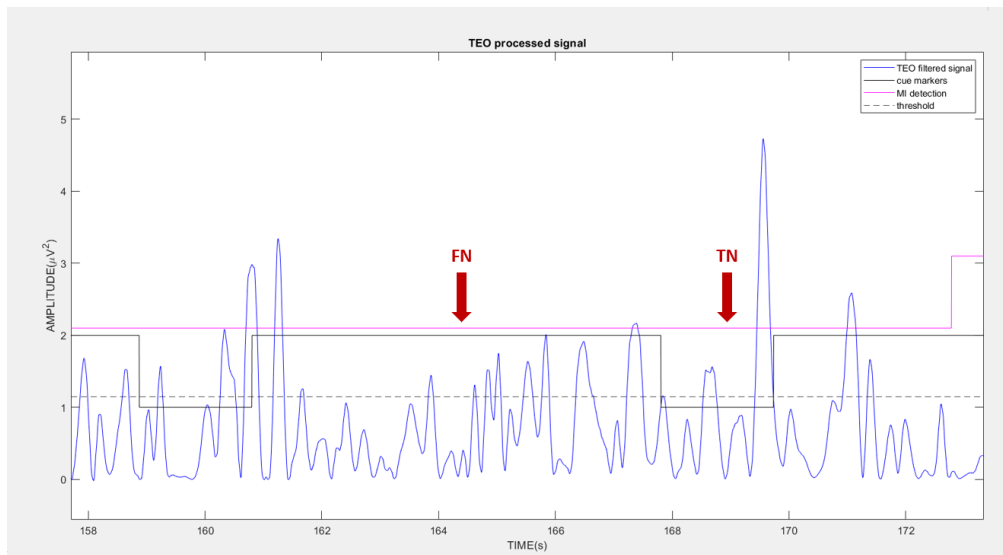


**Figure 5.8:** Example of FP detection from TEO-based signal of Subject 1. The arrows point respectively a FN and a TN.

To perform an analysis of performance of the two implemented techniques, in order to confront them, from Confusion Matrix (CMs), the following metrics were calculated:

- **ACCURACY:** Accuracy indicates the degree of veracity of the test, so it represents how well the system can identify both True Positives and True Negatives [66].

$$Accuracy = \frac{TP + TN}{TP + TN + FP + FN} \quad (5.1)$$

- **PRECISION:**

$$Precision = \frac{TP}{TP + FP} \quad (5.2)$$

- **SENSITIVITY:** Sensitivity is the proportion of true positives correctly identified by the system.

$$Sensitivity = \frac{TP}{TP + FN} \quad (5.3)$$

- **SPECIFICITY:** Specificity is the proportion of true negatives correctly identified by the system, so it indicates how well the system recognizes the periods in which the subjects are not performing motor imagery.

$$Specificity = \frac{TN}{TN + FP} \quad (5.4)$$

- **Activation Delay.** The activation delay (or latency) is defined as the time between the onset of the motor imagery task and the instant when the first event is identified. Keeping the assumption that the subject has the ability to imagine motion when the onset appears, the delay represents the time it

takes the system to recognize the event (Figure 5.9).

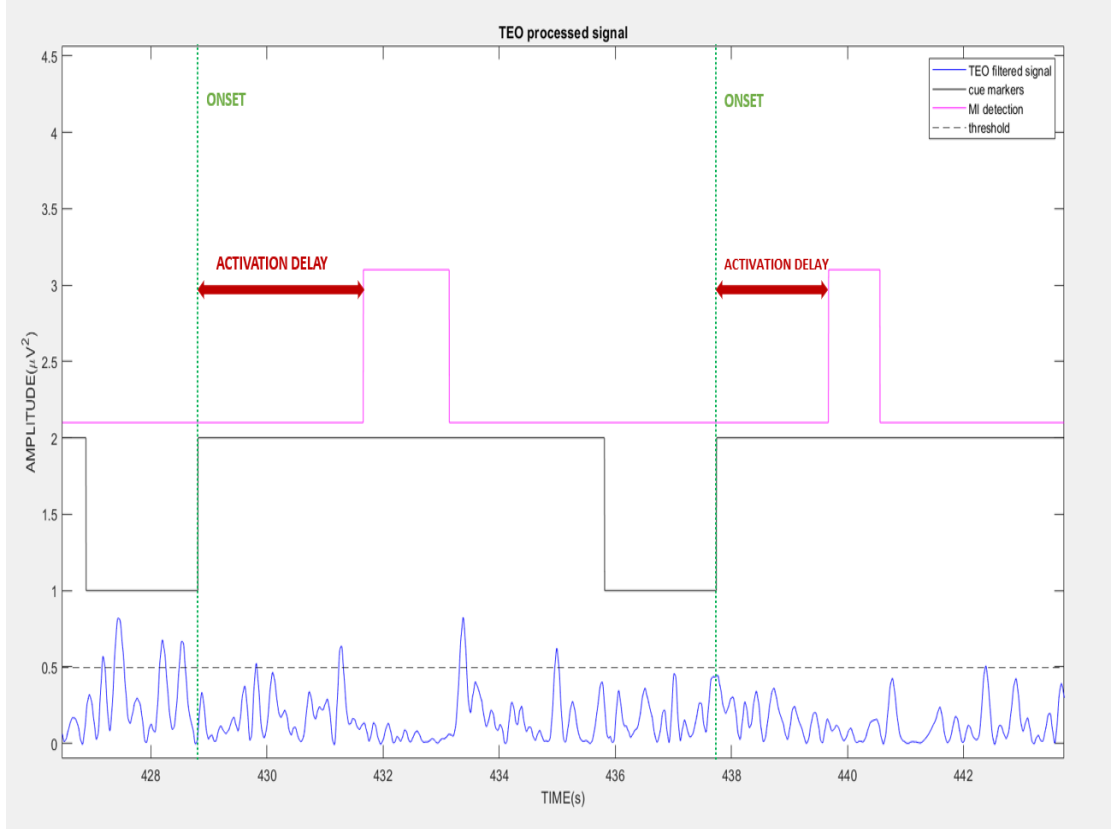


**Figure 5.9:** Example of TP detection from TEO-based signal of Subject 1. The activation delay is defined as the time between the onset of the motor imagery task and the instant when the first event is identified.

## 5.2 PSD and TEO Methods Comparison

In this section, the on-site recorded dataset is referred as Dataset1, while the BCI Competition IV dataset [67] is referred as Dataset2. The acronyms PSD and TEO are used respectively to indicate the PSD-based algorithm and the TEO-based algorithm. The analysis is performed starting from the results obtained using Dataset 1.

	PRECISION (%)		ACCURACY (%)		SENSITIVITY (%)		ACTIVATION DELAY (s)		SPECIFICITY (%)	
	PSD	TEO	PSD	TEO	PSD	TEO	PSD	TEO	PSD	TEO
SUBJECT 1	86.96	85.71	92.5	91.67	100	99	0.7	1.16	85	83.34
SUBJECT 2	76.9	86.88	85	87.5	100	88.33	0.14	1.37	70	86.67
SUBJECT 3	87	98.04	92.4	90.83	99	83.34	0.91	1.89	85	98.33
SUBJECT 4	74.07	76.92	82.5	85	100	99	0.27	0.32	65	70
SUBJECT 5	84.51	81.43	90.8	86.7	100	95	0.02	1.27	81.67	78.3
MEAN	81.89	85.8	88.64	88.34	99.8	92.93	0.41	1.2	77.33	83.33
STD	6.02	7.89	4.6	2.82	0.45	6.91	0.38	0.57	9.25	10.48

**Table 5.1:** Quantitative results for the two algorithms obtained OFFLINE applied on Dataset 1

	PRECISION (%)		ACCURACY (%)		SENSITIVITY (%)		ACTIVATION DELAY (s)		SPECIFICITY (%)	
	PSD	TEO	PSD	TEO	PSD	TEO	PSD	TEO	PSD	TEO
SUBJECT 1	81.08	75.95	88.33	84.17	100	98.9	0.9	1.09	76.67	68.33
SUBJECT 2	77.9	74.07	85.83	82.5	100	100	0.04	0.27	71.7	65
SUBJECT 3	72.29	80.82	80.8	87.5	100	98.33	0.28	0.99	61.7	76.67
SUBJECT 4	71.42	71.43	80	80	99	99.5	0.07	0.22	69	70
SUBJECT 5	75.95	80.82	84.17	87.2	99.5	98.3	0.1	1.36	68.33	76.7
MEAN	75.73	76.62	83.83	84.27	99.7	99.01	0.28	1.31	67.48	69.34
STD	3.99	4.16	3.47	3.18	0.45	0.74	0.36	0.51	5.45	5.2

**Table 5.2:** Quantitative results for the two algorithms obtained ONLINE applied on Dataset 1

As can be seen from the tables (Table 5.1, Table 5.2), both algorithms show good accuracy (Figure 5.10). In particular, both algorithms have a high ability to recognize events as True Positive, as can be deduced from the high sensitivity values. However, the accuracy value is lowered by the presence of False Positives, which are detected less efficiently by both algorithms, as can be seen from the specificity and precision values. The latency (or activation delay) values, are generally lower for the PSD-based algorithm, which demonstrates greater speed in recognizing the subject's motor imagery activity (Figure 5.11).

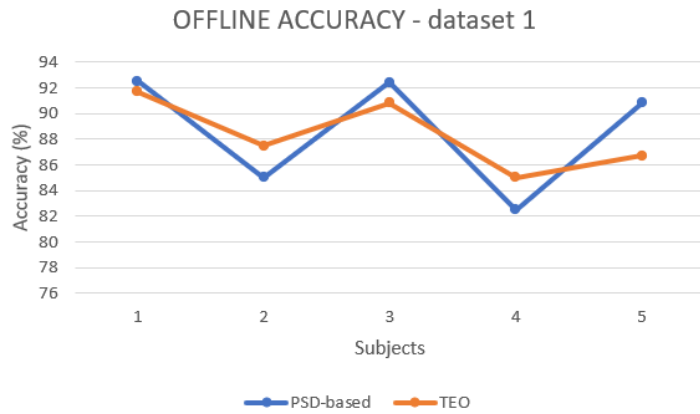


**Figure 5.10:** Both algorithms shows a similar accuracy in recognizing movement intention detection. Accuracy of PSD-based method shows slightly higher inter-subjects variability.

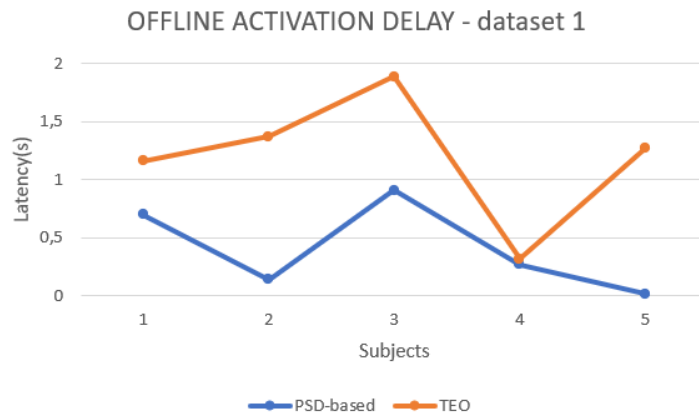


**Figure 5.11:** TEO-based method tends to be slower than PSD-based one in the recognition on the brain activity changes induced by MI task.

In terms of online performances of the systems, PSD-based method shows higher consistency in the results of offline calibrations and online sessions (Figure 5.12), while TEO-based algorithm has averagely higher performances in the movement intention detection offline rather than online (Figure 5.13).

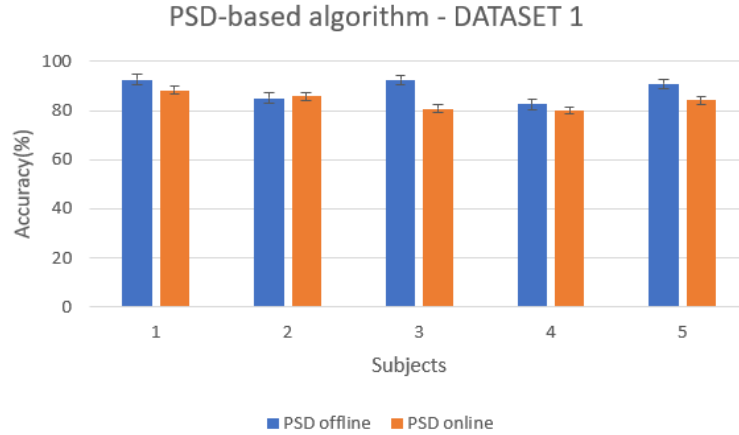


**Figure 5.12:** Accuracy of PSD-based algorithm during offline and online session.

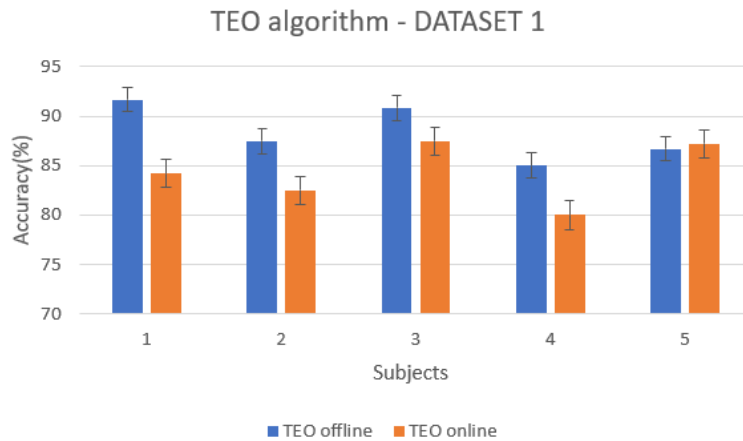


**Figure 5.13:** Accuracy of TEO-based algorithm during offline and online session.

Both algorithms were also tested on Dataset 2 to provide a broader overview of the performance of the implemented systems. The results are shown in Table 5.3 (offline performance) and Table 5.4 (online performance).

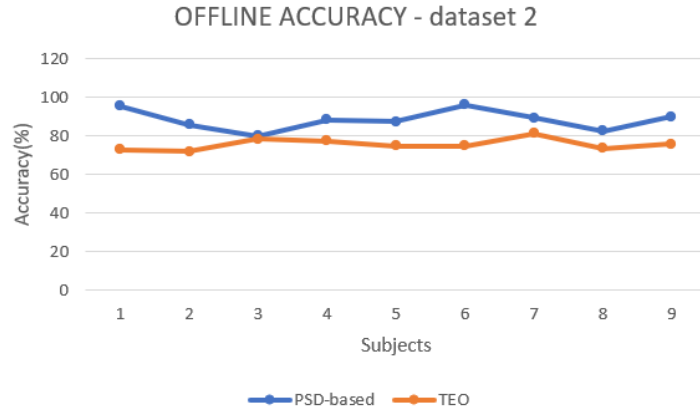
	PRECISION (%)		ACCURACY (%)		SENSITIVITY (%)		ACTIVATION DELAY (s)		SPECIFICITY(%)	
	PSD	TEO	PSD	TEO	PSD	TEO	PSD	TEO	PSD	TEO
SUBJECT 1	91.89	71.96	95.59	73.03	100	75.49	0.47	2.5	91.18	70.59
SUBJECT 2	77.78	78.67	85.7	71.94	100	60.2	0.049	2.8	71.43	83.67
SUBJECT 3	71.43	81.48	80	78.33	100	73.3	0.15	2.4	60	83.33
SUBJECT 4	81.25	84.78	88.46	77.35	100	66.67	0.4	3.1	76.92	88.03
SUBJECT 5	79.85	76.29	87.38	74.76	100	71.84	0.57	2.68	74.76	77.67
SUBJECT 6	92.68	73.75	96.05	75	100	77.63	0.97	2.59	92.1	72.36
SUBJECT 7	82.3	79.13	89.25	81.3	100	85.05	0.74	2.73	78.5	77.57
SUBJECT 8	74.16	73.84	82.58	73.48	100	72.72	0.18	2.63	65.15	74.24
SUBJECT 9	83.49	77.01	90.1	75.82	100	73.62	0.5	2.85	80.22	78
MEAN	81.65	77.43	88.34	75.67	100	72.95	0.45	2.69	76.69	78.38
STD	7.15	4.07	5.32	2.93	0	6.88	0.29	0.21	10.64	5.71

Table 5.3: Quantitative results for the two algorithms obtained OFFLINE applied on Dataset 2

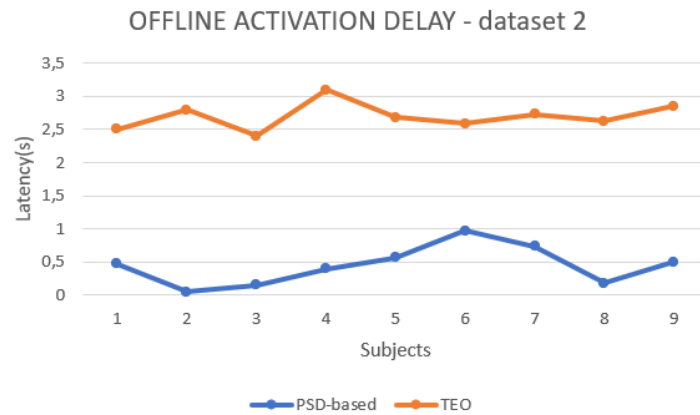
	PRECISION (%)		ACCURACY (%)		SENSITIVITY (%)		ACTIVATION DELAY (s)		SPECIFICITY (%)	
	PSD	TEO	PSD	TEO	PSD	TEO	PSD	TEO	PSD	TEO
SUBJECT 1	90.74	76	94.89	76.53	100	77,55	0.38	1.5	89.79	75.51
SUBJECT 2	75.76	79.73	84	72	100	69	0.19	3.1	85	85
SUBJECT 3	72.13	70	80.68	75.6	100	89,77	0.45	2.4	61.36	61.36
SUBJECT 4	79.63	78.05	87.2	76.74	100	74,41	0.5	3	74.42	79.07
SUBJECT 5	86.3	72.88	88.97	69.85	92.64	63,24	1.08	3.1	85.29	76.47
SUBJECT 6	92.4	76.04	89.41	79.41	85.88	85,9	1.78	2.68	92.94	72.94
SUBJECT 7	77	67.15	85.14	71.17	100	82,88	0.38	2.04	70.27	69.46
SUBJECT 8	74.38	71.7	82.78	73.89	100	78,89	0.21	2.53	65.56	68.89
SUBJECT 9	78.44	74.71	86.26	73.63	100	71,43	0.42	2.74	72.53	75.82
MEAN	80.75	74.02	86.59	74.31	97.61	77	0.59	2.57	77.46	73.84
STD	7.3	3.99	4.2	3.05	5.03	8.45	0.51	0.53	11.16	6.76

Table 5.4: Quantitative results for the two algorithms obtained ONLINE applied on Dataset 2

Results on Dataset 2 shows slightly higher accuracy delivered by PSD-based method (Figure 5.14), and confirms its higher capacity on recognizing the movement intention detection faster than TEO-based one, as can be seen from the activation delay values (Figure 5.15).



**Figure 5.14:** Both algorithms shows a similar accuracy in recognizing movement intention detection. Accuracy of PSD-based is slightly higher than TEO-based one.



**Figure 5.15:** TEO-based shows slower activation delay than PSD-based one in the recognition on the brain activity changes induced by MI task.

As can be seen in Figures 5.16 and 5.17, the considerations previously done about the similar response of offline calibrations and online sessions in terms of accuracy obtained with PSD-based method remain valid, as the TEO-based one shows higher gaps between the two sessions.

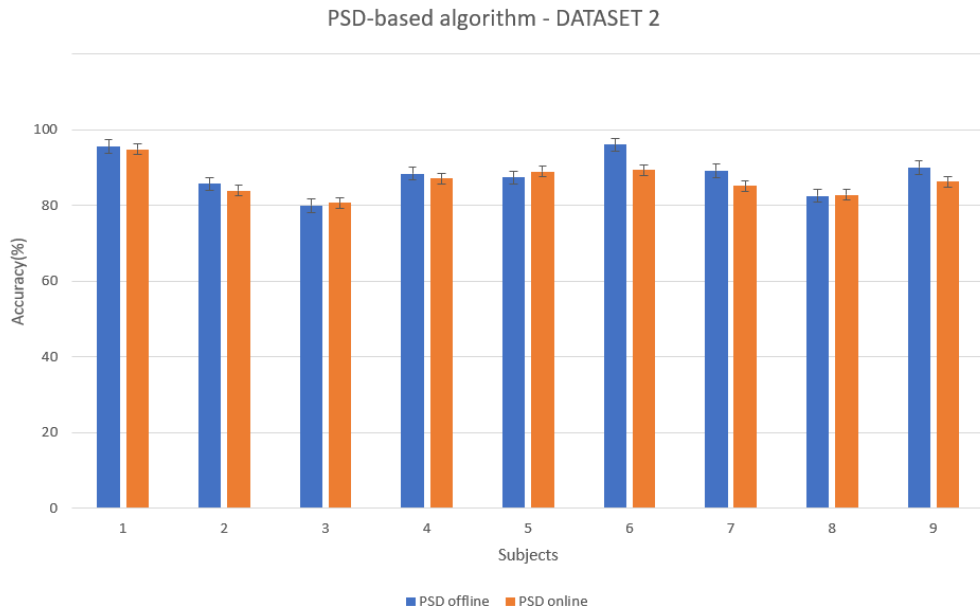


Figure 5.16: Accuracy of PSD-based algorithm during offline and online session.

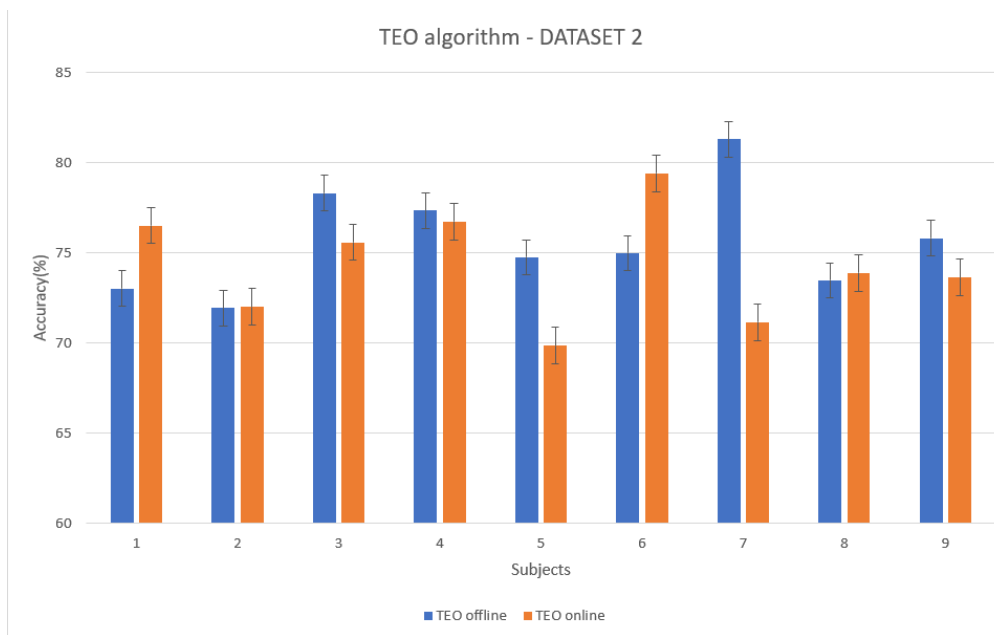
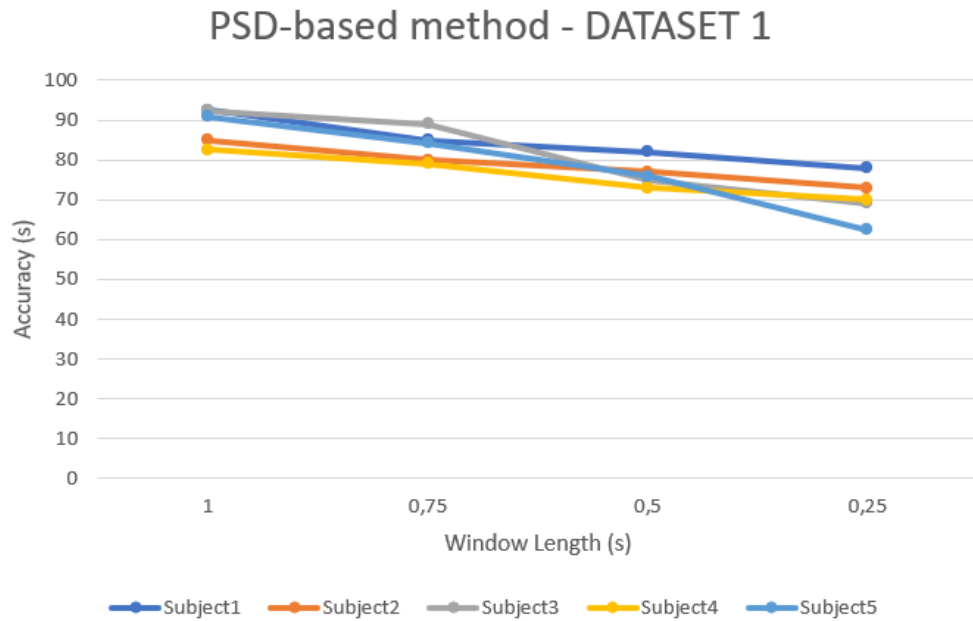


Figure 5.17: Accuracy of TEO-based algorithm during offline and online session.

Overall, PSD-based algorithm has higher accuracy and lower activation delays, but it needs longer computation time, due to the greater amount of processing

that has been done to calculate the PSD and the iterative process implemented to define the threshold. On the other hand, TEO-based technique is faster in terms of computation time, because it has a less complex implementation and the observation window used to detect the movement intention has a length of 300 ms, versus the 1 second window length used in the PSD-based method. In order to decrease the time requested to the PSD algorithm to compute, the window length can be shortened, at expense of the accuracy delivered by the system, as can be seen in Figure 5.18.



**Figure 5.18:** Accuracy of PSD-based algorithm obtained for different observation window lengths.

## Chapter 6

# Conclusion and Future Perspective

In this thesis project, EEG signal was investigated for the purpose of being used for the development of an EEG-based BCI system. The EEG signal exhibits various responses to internal and external stimuli, which can be analyzed to extract parameters useful for external applications, such as FES control. In particular, variations in the signal induced by motor imagery can be employed to develop a powerful rehabilitation tool that associates the cortical activation occurring during movement imagery and the visual and sensory feedback of movement induced by FES. In this context, two approaches for motor intention recognition have been developed, to be used to provide accurate inputs for FES activation in a BCI system. The proposed algorithms process EEG signals recorded during motor imagery tasks in the mu/alpha frequency band, where the oscillations changes due to the activation of motor-related brain regions are more obvious. EEG signal was recorded on-site using g.tec system. Five subjects participated to the recordings, during which they were instructed to perform motor imagery of right and left hand, following a predefined paradigm. Two sessions per subject were recorded, to be used respectively for an offline calibration and a simulated online test session. The signals employed in the developing of the algorithms were acquired from a single EEG channel, placed over the central region of the scalp. After preprocessing the signal using a notch filter and a highpass filter, a time-frequency analysis was performed for each subject, to identify the frequency range and the cortical region in which was more noticeable the brain activity during motor imagery. In this way it was possible to determine the best conditions to easily detect the movement intention. Both algorithms exploit a time-controlled threshold method, that recognizes the movement intention by detecting changes in cortical fluctuation during motor imagery. The first algorithm performs a signal analysis in the frequency domain,

using as main parameter the Power Spectral Density (PSD), which shows amplitude suppression during motor imagination. The second algorithm detects the energy changes in the EEG signal processed by Teager's Energy Operator (TEO). The two different approaches were tested on the on-site recorded dataset and on the one provided by BCI competition IV, then the performance of the systems were evaluated in terms of sensitivity, specificity, accuracy, precision and activation delay. Both methods have shown a high sensitivity in recognizing the movement intention. PSD-based method exhibits good accuracy in both datasets and fast recognition of the movement intention, compared with TEO-based technique. However, the Teager operator approach was investigated because, being defined in the continuous domain, it is potentially usable for nonstandard BCI applications. The typical structure of a BCI involves acquisition of the EEG signal, conversion to a digital signal performed by an ADC, and transmission of the data to a device (e.g., computer). The theoretical aspect of the implemented algorithm suggests that TEO could be applied directly on the analog signal, as it extracts the energy content using a linear combination of signal derivatives. Potentially, then, a device that apply a hardware version of TEO could be implemented, that employes hardware derivative and uses a voltage comparator to detect the events of interest. This could lead to the development of an hardware acquisition system that does not require the use of an ADC and outputs motor intention events directly. The literature suggests little insight into the feasibility of such an implemented system, because it generally relies on a traditional implementation. It might be an interesting future work to investigate the performance and cost of a system built in a nontypical manner. Besides of that, future works should focus on executing online tests of both systems using FES, to further increase the performances of the implemented methods. Studies have demonstrated that providing a feedback by means of FES helps the subjects to better perform motor imagery and potentially allows faster detection of the motor intention.

# Bibliography

- [1] Deanna M Thompson, Abigail N Koppes, John G Hardy, and Christine E Schmidt. «Electrical stimuli in the central nervous system microenvironment». In: *Annu. Rev. Biomed. Eng* 16.1 (2014), pp. 397–430 (cit. on p. 1).
- [2] <https://www.msmanuals.com/home/multimedia/table/how-the-spine-is-organized> (cit. on p. 2).
- [3] Zerina Tomkins. *Applied Anatomy & Physiology: an interdisciplinary approach*. Elsevier Health Sciences, 2019 (cit. on pp. 2, 3).
- [4] Laura A Freberg. *Psicologia biologica*. Zanichelli, 2007 (cit. on pp. 2, 6, 9).
- [5] Jürgen K Mai and George Paxinos. *The human nervous system*. Academic press, 2011 (cit. on p. 2).
- [6] Jonathan R Wolpaw and E Winter Wolpaw. «Brain-computer interfaces: something new under the sun». In: *Brain-computer interfaces: principles and practice* 14 (2012) (cit. on pp. 3, 5, 18, 19).
- [7] Giorgia Bussu. *Attentional Modulation Effects on Brain Networks: an fMRI Study on the Visual Attention Network and the Default-Mode Network*. Aug. 2015. DOI: 10.13140/RG.2.2.16094.87362 (cit. on p. 3).
- [8] <https://bodell.mtchs.org/OnlineBio/BI0CD/text/chapter28/concept28.4.html> (cit. on p. 4).
- [9] <https://epomedicine.com/medical-students/cerebral-cortex-layers-microanatomy-simplified/> (cit. on p. 5).
- [10] Federico Carpi, Danilo De Rossi, and Fenomeni Bioelettrici. «Potenziali elettroencefalografici e potenziali evocati». In: () (cit. on pp. 5, 12, 16).
- [11] *Introduction to the Central Nervous System*. <https://legacy.cnx.org/content/m62520/1.1/> (cit. on pp. 6–11).
- [12] Roger Carpenter and Benjamin Reddi. *Neurophysiology: a conceptual approach*. CRC Press, 2012 (cit. on p. 7).
- [13] Guido Avanzolini and Elisa Magosso. *Strumentazione biomedica: progetto e impiego dei sistemi di misura*. Pàtron, 2015 (cit. on pp. 10, 17, 21).

- [14] Hans Hallez et al. «Review on solving the forward problem in EEG source analysis». In: *Journal of neuroengineering and rehabilitation* 4.1 (2007), pp. 1–29 (cit. on p. 11).
- [15] Seyed Farhad Abtahi. «Feasibility of fetal EEG Recording». MA thesis. 2012 (cit. on p. 11).
- [16] Paulo Aguiar, Andre David, Sandra Paulo, and Agostinho Rosa. «EEG-SOLVER—brain activity and genetic algorithms». In: *Proceedings of the 2000 ACM symposium on Applied computing-Volume 1*. 2000, pp. 80–84 (cit. on p. 12).
- [17] Sebastianus Petrus van den Broek, F Reinders, M Donderwinkel, and MJ Peters. «Volume conduction effects in EEG and MEG». In: *Electroencephalography and clinical neurophysiology* 106.6 (1998), pp. 522–534 (cit. on p. 12).
- [18] Chetan S Nayak and Arayamparambil C Anilkumar. *EEG Normal Waveforms. StatPearls*. 2020 (cit. on pp. 13, 15).
- [19] Priyanka A Abhang, Bharti W Gawali, and Suresh C Mehrotra. «Technological basics of EEG recording and operation of apparatus». In: *Introduction to EEG-and Speech-Based Emotion Recognition* (2016), pp. 19–50 (cit. on p. 13).
- [20] Mila Halgren et al. «The generation and propagation of the human alpha rhythm». In: *Proceedings of the National Academy of Sciences* 116.47 (2019), pp. 23772–23782 (cit. on pp. 13, 14).
- [21] Maria Roberta Cilio and Francesco Pisani. «Electroencephalography in the Preterm and Term Infant». In: *Fetal and Neonatal Physiology*. Elsevier, 2017, pp. 1362–1389 (cit. on p. 13).
- [22] Gert Pfurtscheller. «Functional brain imaging based on ERD/ERS». In: *Vision research* 41.10-11 (2001), pp. 1257–1260 (cit. on pp. 14, 18, 19, 28).
- [23] Piotr Wierzgała, Dariusz Zapała, Grzegorz M Wojcik, and Jolanta Masiak. «Most popular signal processing methods in motor-imagery BCI: a review and meta-analysis». In: *Frontiers in neuroinformatics* 12 (2018), p. 78 (cit. on p. 14).
- [24] Yanan Sui et al. «Deep brain stimulation initiative: toward innovative technology, new disease indications, and approaches to current and future clinical challenges in neuromodulation therapy». In: *Frontiers in Neurology* 11 (2021), p. 1706 (cit. on p. 14).
- [25] Gianluca Di Flumeri, Pietro Aricò, Gianluca Borghini, Nicolina Sciaraffa, Antonello Di Florio, and Fabio Babiloni. «The dry revolution: Evaluation of three different EEG dry electrode types in terms of signal spectral features, mental states classification and usability». In: *Sensors* 19.6 (2019), p. 1365 (cit. on p. 15).

- [26] FCGE Sharbrough. «American Electroencephalographic Society guidelines for standard electrode position nomenclature». In: *J clin Neurophysiol* 8 (1991), pp. 200–202 (cit. on p. 15).
- [27] JAAKKO Malmivuo and ROBERT Plonsey. «Bioelectromagnetism. 13. Electroencephalography». In: *Principles and Applications of Bioelectric and Biomagnetic Fields* (1995), p. 247 (cit. on p. 16).
- [28] Junaid Ahmed. «Brain Machine Interface using EEG Sci-fi to Reality Neural Interface Engineering Brain Machine Interface using EEG 1 BRAIN MACHINE INTERFACE USING EEG». In: (Dec. 2016) (cit. on p. 16).
- [29] Han Yuan and Bin He. «Brain–computer interfaces using sensorimotor rhythms: current state and future perspectives». In: *IEEE Transactions on Biomedical Engineering* 61.5 (2014), pp. 1425–1435 (cit. on p. 19).
- [30] Samar Hamid and Ray Hayek. «Role of electrical stimulation for rehabilitation and regeneration after spinal cord injury: an overview». In: *European Spine Journal* 17.9 (2008), pp. 1256–1269 (cit. on p. 20).
- [31] Amjed S Al-Fahoum and Ausilah A Al-Fraihat. «Methods of EEG signal features extraction using linear analysis in frequency and time-frequency domains». In: *International Scholarly Research Notices 2014* (2014) (cit. on p. 21).
- [32] Vangelis P Oikonomou, Kostas Georgiadis, George Liaros, Spiros Nikolopoulos, and Ioannis Kompatsiaris. «A comparison study on EEG signal processing techniques using motor imagery EEG data». In: *2017 IEEE 30th international symposium on computer-based medical systems (CBMS)*. IEEE. 2017, pp. 781–786 (cit. on p. 21).
- [33] Maria Laura Manca and Luigi Murri. «Fourier ed il ruolo della sua trasformata nella ricerca neurologica». In: *Dipartimento di Neuroscienze, Università di Pisa* () (cit. on p. 22).
- [34] Stanisław Solnik, Paul DeVita, Patrick Rider, Benjamin Long, and Tibor Hortobágyi. «Teager–Kaiser Operator improves the accuracy of EMG onset detection independent of signal-to-noise ratio». In: *Acta of bioengineering and biomechanics/Wroclaw University of Technology* 10.2 (2008), p. 65 (cit. on p. 22).
- [35] James F Kaiser. «On a simple algorithm to calculate the ‘energy’ of a signal». In: *International conference on acoustics, speech, and signal processing*. IEEE. 1990, pp. 381–384 (cit. on pp. 22, 23, 40).
- [36] Hamed Beyramienanlou and Nasser Lotfivand. «An efficient teager energy operator-based automated QRS complex detection». In: *Journal of healthcare engineering* 2018 (2018) (cit. on p. 23).

- [37] James F Kaiser. «Some useful properties of Teager’s energy operators». In: *1993 IEEE international conference on acoustics, speech, and signal processing*. Vol. 3. IEEE. 1993, pp. 149–152 (cit. on p. 23).
- [38] Muhammad Ahmed Khan, Rig Das, Helle K Iversen, and Sadasivan Puthusserypady. «Review on motor imagery based BCI systems for upper limb post-stroke neurorehabilitation: From designing to application». In: *Computers in Biology and Medicine* 123 (2020), p. 103843 (cit. on pp. 24, 25).
- [39] Gert Pfurtscheller, Bernhard Graimann, and Christa Neuper. «EEG-Based Brain-Computer Interface System». In: *Wiley Encyclopedia of Biomedical Engineering* (2006) (cit. on p. 24).
- [40] Colin M McCrimmon, Christine E King, Po T Wang, Steven C Cramer, Zoran Nenadic, and An H Do. «Brain-controlled functional electrical stimulation for lower-limb motor recovery in stroke survivors». In: *2014 36th Annual International Conference of the IEEE Engineering in Medicine and Biology Society*. IEEE. 2014, pp. 1247–1250 (cit. on p. 25).
- [41] Aleksandra Vuckovic, Leslie Wallace, and David B Allan. «Hybrid brain-computer interface and functional electrical stimulation for sensorimotor training in participants with tetraplegia: a proof-of-concept study». In: *Journal of neurologic physical therapy* 39.1 (2015), pp. 3–14 (cit. on pp. 25, 26, 33, 51).
- [42] Li-Wei Ko, SSK Ranga, Oleksii Komarov, and Chung-Chiang Chen. «Development of single-channel hybrid BCI system using motor imagery and SSVEP». In: *Journal of healthcare engineering* 2017 (2017) (cit. on p. 26).
- [43] Maryam Mahmoodi, Bahador Makkiabadi, Mehran Mahmoudi, and Saeid Sanei. «A new method for accurate detection of movement intention from single channel EEG for online BCI». In: *Computer Methods and Programs in Biomedicine Update* 1 (2021), p. 100027 (cit. on p. 26).
- [44] <https://www.gtec.at/product/gnutilus-research/> (cit. on p. 27).
- [45] Selina C Wriessnegger, Gernot R Müller-Putz, Clemens Brunner, and Andreea I Sburlea. «Inter-and intra-individual variability in brain oscillations during sports motor imagery». In: *Frontiers in Human Neuroscience* 14 (2020), p. 576241 (cit. on p. 28).
- [46] Alessandro B Benevides, Teodiano F Bastos Filho, and Mário Sarcinelli Filho. «Comparison of artifact removal techniques on single-trial event-related potentials for use in brain-computer interfaces». In: *CEP* 48 (2013), p. 08 (cit. on p. 29).

- [47] Izabela Rejer and Pawel Górski. «Benefits of ICA in the case of a few channel EEG». In: *2015 37th Annual International Conference of the IEEE Engineering in Medicine and Biology Society (EMBC)*. IEEE. 2015, pp. 7434–7437 (cit. on p. 31).
- [48] M Ungureanu, C Bigan, R Strungaru, V Lazarescu, et al. «Independent component analysis applied in biomedical signal processing». In: *Measurement Science Review* 4.2 (2004), p. 18 (cit. on p. 32).
- [49] Raquib-ul Alam, Haifeng Zhao, Andrew Goodwin, Omid Kavehei, and Alistair McEwan. «Differences in power spectral densities and phase quantities due to processing of eeg signals». In: *Sensors* 20.21 (2020), p. 6285 (cit. on p. 33).
- [50] Vangelis P Oikonomou, Georgios Liaros, Kostantinos Georgiadis, Elisavet Chatzilari, Katerina Adam, Spiros Nikolopoulos, and Ioannis Kompatsiaris. «Comparative evaluation of state-of-the-art algorithms for SSVEP-based BCIs». In: *arXiv preprint arXiv:1602.00904* (2016) (cit. on p. 33).
- [51] <https://sapienlabs.org/lab-talk/factors-that-impact-power-spectrum-density-estimation/> (cit. on p. 34).
- [52] Andreas Widmann, Erich Schröger, and Burkhard Maess. «Digital filter design for electrophysiological data—a practical approach». In: *Journal of neuroscience methods* 250 (2015), pp. 34–46 (cit. on p. 38).
- [53] Michał Lewandowski and Janusz Walczak. «Comparison of single-level and multi-level filtering systems of EEG signal». In: *2015 Signal Processing: Algorithms, Architectures, Arrangements, and Applications (SPA)*. IEEE. 2015, pp. 34–37 (cit. on p. 38).
- [54] Hong Zeng, Aiguo Song, Ruqiang Yan, and Hongyun Qin. «EOG artifact correction from EEG recording using stationary subspace analysis and empirical mode decomposition». In: *Sensors* 13.11 (2013), pp. 14839–14859 (cit. on p. 39).
- [55] Xiao Jiang, Gui-Bin Bian, and Zean Tian. «Removal of artifacts from EEG signals: a review». In: *Sensors* 19.5 (2019), p. 987 (cit. on p. 39).
- [56] Aykut Erdamar, Fazıl Duman, and Sinan Yetkin. «A wavelet and teager energy operator based method for automatic detection of K-Complex in sleep EEG». In: *Expert Systems with Applications* 39.1 (2012), pp. 1284–1290 (cit. on p. 40).
- [57] I Antoniadou, G Manson, N Dervilis, T Barszcz, WJ Staszewski, and K Worden. «Use of the Teager-Kaiser energy operator for condition monitoring of a wind turbine gearbox». In: *International conference on noise and vibration engineering*. 2012, pp. 4255–4268 (cit. on p. 40).

- [58] Petros Maragos, James F Kaiser, and Thomas F Quatieri. «Energy separation in signal modulations with application to speech analysis». In: *IEEE transactions on signal processing* 41.10 (1993), pp. 3024–3051 (cit. on p. 40).
- [59] Pradeep Kr Banerjee and Nirmal B Chakrabarti. «Noise sensitivity of Teager-Kaiser energy operators and their ratios». In: *2015 International Conference on Advances in Computing, Communications and Informatics (ICACCI)*. IEEE. 2015, pp. 2265–2271 (cit. on p. 42).
- [60] Mareike Daeglau, Catharina Zich, Julius Welzel, Samira Kristina Saak, Jannik Florian Scheffels, and Cornelia Kranczioch. «Event-related desynchronization in motor imagery with EEG neurofeedback in the context of declarative interference and sleep». In: *Neuroimage: Reports* 1.4 (2021), p. 100058 (cit. on p. 42).
- [61] Yongwoong Jeon, Chang S Nam, Young-Joo Kim, and Min Cheol Whang. «Event-related (De) synchronization (ERD/ERS) during motor imagery tasks: Implications for brain–computer interfaces». In: *International Journal of Industrial Ergonomics* 41.5 (2011), pp. 428–436 (cit. on p. 52).
- [62] Gert Pfurtscheller. «Spatiotemporal ERD/ERS patterns during voluntary movement and motor imagery». In: *Supplements to Clinical neurophysiology* 53 (2000), pp. 196–198 (cit. on p. 52).
- [63] Christa Neuper, Michael Wörtz, and Gert Pfurtscheller. «ERD/ERS patterns reflecting sensorimotor activation and deactivation». In: *Progress in brain research* 159 (2006), pp. 211–222 (cit. on p. 53).
- [64] Cecilia L Maeder, Claudia Sannelli, Stefan Haufe, and Benjamin Blankertz. «Pre-stimulus sensorimotor rhythms influence brain–computer interface classification performance». In: *IEEE Transactions on neural systems and rehabilitation engineering* 20.5 (2012), pp. 653–662 (cit. on p. 53).
- [65] Karim Fifel. «Readiness potential and neuronal determinism: new insights on Libet experiment». In: *Journal of Neuroscience* 38.4 (2018), pp. 784–786 (cit. on p. 53).
- [66] Wen Zhu, Nancy Zeng, Ning Wang, et al. «Sensitivity, specificity, accuracy, associated confidence interval and ROC analysis with practical SAS implementations». In: *NESUG proceedings: health care and life sciences, Baltimore, Maryland* 19 (2010), p. 67 (cit. on p. 55).
- [67] R Leeb, C Brunner, G Müller-Putz, A Schlögl, and G Pfurtscheller. «BCI Competition 2008–Graz data set B». In: *Graz University of Technology, Austria* (2008), pp. 1–6 (cit. on p. 56).